

Elevated atmospheric CO₂ concentration and vegetation structural changes contributed to GPP increase more than climate and forest cover changes in subtropical forests of China

5 Tao Chen^{1,2,*}, Félicien Meunier², Marc Peaucelle³, Guoping Tang^{1,*}, Ye Yuan⁴, Hans Verbeeck²

1. Carbon-Water Research Station in Karst Regions of Northern Guangdong, School of Geography and Planning, Sun Yat-Sen University, Guangzhou 510006, China

2. CAVElab – Computational and Applied Vegetation Ecology, Department of Environment, Ghent University, Ghent 9000, Belgium

10 3. INRAE, Université de Bordeaux, UMR 1391 ISPA, 33140 Villenave-d’Ornon, France

4. State Key Laboratory of Desert and Oasis Ecology, Xinjiang Institute of Ecology and Geography, Chinese Academy of Sciences, Urumqi 830011, China

*Corresponding to: Tao Chen (chent265@mail2.sysu.edu.cn); Guoping Tang (tanggp3@mail.sysu.edu.cn)

Abstract: The subtropical forests ~~is gross primary productivity (GPP)~~ play a pivotal role in the global carbon cycle and in regulating the global climate. Quantifying the individual and combined effects of forest cover change (FCC), vegetation structural change (~~VSC~~, i.e., leaf area index (LAI)), CO₂ fertilization, and climate change (CC) on annual ~~gross primary productivity (GPP)~~ **GPP** dynamics of various subtropical forest types are essential for mitigating carbon emissions and predicting **future** climate changes, but these impacts remain unclear. In this study, we used a process-based model to comprehensively investigate the impacts of these factors on GPP variations with a series of model experiments in China’s subtropical forests during 2001-2018. Simulated ~~actual~~ GPP showed a significant increasing trend (~~20.67 gC/m²/year~~ **26.72 TgC year⁻¹**, $p < 0.001$) under the interaction effects of **FCC**, **LAI change**, **rising CO₂** and **CC** ~~these factors~~. The CO₂ fertilization (~~6.84 gC/m²/year~~ **8.23 TgC year⁻¹**, $p < 0.001$) and ~~VSC-LAI change~~ (~~3.79 gC/m²/year~~, $p = 0.004$ **4.55 TgC year⁻¹**, $p = 0.005$) were the two dominant drivers of total subtropical forest GPP increase, followed by the effect of FCC (~~0.52 gC/m²/year~~, $p < 0.001$ **1.35 TgC year⁻¹**, $p < 0.001$) and CC (~~0.92 gC/m²/year~~ **1.11 TgC year⁻¹**, $p = 0.08$). We observed different responses to drivers depending on forest types. The evergreen broadleaved forests have a high carbon sink potential due to the positive effects of all drivers. Both the FCC (~~0.19 gC/m²/year~~, $p < 0.051$ **0.29 TgC year⁻¹**, $p < 0.001$) and CC (~~1.22 gC/m²/year~~, $p < 0.050$ **0.53 TgC year⁻¹**, $p < 0.05$) significantly decreased evergreen needleleaved forest GPP, while their negative effects were almost offset by the positive impact of **VSC LAI changes**. Our results indicated that **forest structural change LAI** outweighed the ~~forest cover change~~ **FCC** in promoting GPP, which is an **overlooked-essential** driver that needs to be accounted for in studies, as well as ecological and management programs. Overall, our study offers a novel perspective on different drivers of subtropical forest GPP changes, ~~which and~~ provides valuable information for policy makers ~~in~~ **to better manage subtropical forests management** to mitigate climate

change risks.

Keywords: Subtropical forests, Gross primary production (GPP), Vegetation structure change, Climate change, BEPS process-based model

Abbreviations: BEPS, the Boreal Ecosystem Productivity Simulator; GPP, Gross primary productivity; FCC, Forest cover change; LAI, Leaf area index; CC, Climate change; CO₂, Carbon dioxide; EBF, Evergreen broadleaved forest; ENF, Evergreen needle-leaved forest; DBF, Deciduous broadleaved forest; MXF, Mixed forest; QYZ, Qianyanzhou station; DHS, Dinghushan station; ALS, Ailaoshan station; V_{cmax}, the maximum carboxylation rate; NEP, Net ecosystem productivity; ER, Ecosystem respiration.

1. Introduction

Terrestrial ecosystems can capture carbon dioxide (CO₂) from the atmosphere through photosynthesis, which is regarded as a potential solution for slowing down the increase in global CO₂ concentration (Keenan et al., 2016) and mitigating global warming (Fang et al., 2018; Shevliakova et al., 2013). ~~Mitigating emissions through ecosystem carbon absorption is a potential solution to slow the increase of global atmospheric carbon dioxide (CO₂) concentration and temperature (Fang et al., 2014).~~

Forest ecosystems, which cover about 30% of the global land area (Thornton et al., 2002) (Forzieri et al., 2022), are one of the main terrestrial carbon sinks (Mathias and Trugman, 2022; Pan et al., 2011) through photosynthesis (Beer et al., 2010). China's forest ecosystems, with an area of approximately 1.95×10^6 km² (Li et al., 2014), are mainly distributed in the subtropical regions, which are an important component of the global forest ecosystems and crucial to the global and regional climate system (Fang et al., 2010; Yu et al., 2014). However, China is still one of the world's top emitters of greenhouse gases that directly contribute to global warming (Friedlingstein et al., 2022; Yu et al., 2014). GPP is an important indicator reflecting the ecosystem carbon sequestration capacity, which drives terrestrial carbon sequestration and partially offsets anthropogenic CO₂ emissions. Therefore, precise quantification of China's subtropical forest GPP and understanding of its driving mechanisms are of great importance for scientists and policy makers to mitigate climate change and carbon emissions with the carbon sink potential of the Chinese subtropical forests (Fang et al., 2010; Yu et al., 2014).

Several national key ecological restoration programs have been implemented in China to reverse land and environmental degradation (Lu et al., 2018). ~~such as~~ As a result, the natural and planted forest area increased by 2.3×10^7 ha and 2.6×10^7 ha during the past two decades, respectively (Chen et al., 2021b). Remote sensing observations have also identified the hotspots of forest gains and greening in southern China resulting from these programs' implements (Chen et al., 2019a; Tong et al., 2018). However, the subtropical regions are the most developed in China and have a very high population density with more than 10% (approximately ~~8.20.82~~ billion) of the world population. Intense land cover/use changes have become prominent in this region due to rapid industrialization and urbanization, leading to serious changes to forest ecosystems (e.g., LAI and GPP) (Chen et al., 2019b; Tong et al., 2018; Zhang et al., 2014). Previous studies reported that LAI was the important biotic driver of carbon sink increase in China's forest ecosystems ~~VSC can reflect the vegetation growth and land use management~~ (Chen et al., 2019a; Chen et al., 2019b). Especially, LAI is a critical parameter for depicting

75 vegetation canopy structure, which can influence some important photosynthetic parameters (e.g.,
quantum yield (α), diurnal ecosystem respiration rate (R_d), etc.), and in particular, it can determine the
amount of photosynthetically active sunlight that is absorbed by vegetation and thus influence
photosynthetic assimilation rate (Piao et al., 2020). In addition, LAI can influence the annual productivity
of vegetation by ruling the length of the growing season (i.e., phenology). Meanwhile, the annual mean
80 (e.g., 407 ppm in 2017) (CMA, 2018). Elevated CO₂ concentrations may enrich the intercellular CO₂
content and thus enhance the photosynthetic rates and plant productivity (i.e., GPP) at the ecosystem
scale, which is known as the CO₂ fertilization effect (Piao et al., 2020). The CO₂ fertilization was also
identified as the pivotal driver for enhancing carbon sink in terrestrial ecosystems, and some studies even
85 reported that the southern region of China was more affected by the CO₂ fertilization effect than other
Chinese regions (Chen et al., 2019b; Zhu et al., 2016), which also affected the photosynthetic rates, and
thereby influenced the vegetation productivity (Chen et al., 2022a).

In addition to these drivers, the annual mean temperature in the Chinese subtropical monsoon
region has increased by more than 1.0 °C over the past 30 years ~~the annual mean temperature in the~~
~~Chinese subtropical monsoon region has increased by more than 1.0 °C over the past 30 years, which~~
90 ~~was higher than the global average~~ (Fang et al., 2018), ~~which was higher than the global surface~~
~~temperature increase~~ (Sun et al., 2019) and ~~has also~~ influenced the forest carbon uptake (Gao et al., 2017;
Yuan et al., 2016). Recently, several studies investigated the roles of climate factors in regulating ~~the~~
~~changes of~~ forest GPP changes at the site or global scales (Barman et al., 2014; Ma et al., 2015), as well
95 as in some regions of China (Ma et al., 2019; Yao et al., 2018b). For instance, previous studies showed
that temperature was the major factor influencing GPP variations in the Yangtze River Basin of southern
China (Nie et al., 2023), as well as in other southern parts of China (Ma et al., 2019). Generally, a proper
increasing temperature can promote enzyme activity and CO₂ fixation (Siddik et al., 2019; Moore, et al.,
2021). However, when the temperature increases exceed the optimal temperature, the activity of enzymes
in plants will decrease, thereby affecting the photosynthesis rate and carbon sequestration. Climate
100 warming can also increase the vapor pressure deficit (VPD), leading to more drought stress on plants
(Yuan et al., 2019). When atmospheric moisture is insufficient, plants tend to inhibit photosynthesis by
reducing stomatal conductance, thereby significantly reducing GPP (Yuan et al., 2019; Grossiord et al.,
2020). Besides, Li et al., (2022) highlighted that precipitation dominated the interannual changes in forest
GPP in Southwest China, while vegetation productivity response to precipitation variations shows large
105 spatial heterogeneity (Camberlin et al., 2007), which largely depends on topographic attributes,
vegetation types, and even soil texture. Additionally, a previous study also indicated that the GPP changes
were more affected by solar radiation than by precipitation and temperature in humid region of China
(Chen et al., 2021a). Therefore, the changes in GPP in response to different climatic factors can be both
positive and negative across different regions and periods. Some studies indicated that temperature was
110 the major factor in forest GPP variations, while other studies suggested that precipitation and solar
radiation were the key driving forces (Chen et al., 2021a; Fyllas et al., 2017; Li et al., 2022; Mo et al.,
2018). Moreover, and CO₂ fertilization were the pivotal drivers for enhancing carbon sink in terrestrial
vegetation, particularly of China's forest ecosystems (Chen et al., 2019b; Chen et al., 2021a). Therefore,

115 the dominant factors affecting GPP varied a lot depending on regions and different time scales, and thus
these studies in identifying the drivers of changes in GPP led to divergent conclusions. Moreover, some
of the recent studies~~most of the current studies~~ mainly considered different forests as a single forest type,
and attempted to untangle the individual and combined impact of different factors on forest GPP changes
(Chen et al., 2021a; Zhang et al., 2022). However, the relative contributions of these factors to China's
subtropical forest GPP variations for specific forest types were still not clear.

120 In the past decades, different methods have been used to estimate vegetation GPP. The process-
based models, especially in combination with remote sensing data (Chen et al., 2019b; Liu et al., 1997),
are by far one of the most important tools for different forests by explicitly representing processes and
their interaction with the environment and for disentangling the drivers of GPP variations over multiple
125 spatiotemporal scales. The Boreal Ecosystem Productivity Simulator (BEPS) was developed based on
the FOREST-BGC model (Running and Coughlan, 1988), which is a process-based diagnostic model
and has the advantages of incorporating ~~the~~ remote sensing data (e.g., LAI and land cover type) to
represent the solid biophysical processes. Recently, the BEPS model has been widely used to simulate
carbon fluxes at the regional and global scales~~Recently, the BEPS model has been widely used at the~~
~~regional and global scale and proved to be one of the better performing models for forest GPP simulations~~
130 (Chen et al., 2019b; Chen et al., 2012; Liu et al., 1997; Luo et al., 2019; Wang et al., 2021a). Although,
it has been well evaluated and validated in China~~especially it has been well evaluated and validated in~~
~~China~~ (Feng et al., 2007; Liu et al., 2018; Peng et al., 2021; Wang et al., 2018), it-but has not been used
to unravel the drivers of different forests changes.

Therefore, in this study, we especially focus on the subtropical forest ecosystems of China. The
135 BEPS model was used to simulate different forest GPP. The specific objective of this study is to (1) test
the performance of the BEPS model in simulating ~~the~~ GPP of the China's subtropical forest ecosystems,
(2) quantify the spatiotemporal trends in GPP of different forest types across the subtropics~~quantify~~
~~spatiotemporal trends in different GPP across the subtropical forests~~, and (3) disentangle the relative
effects of ~~the~~ forest cover change, climate change, LAI~~vegetation structure change~~, and CO₂ fertilization
140 on different forest GPP variations in the study area. ~~The results of this study may provide valuable~~
~~information for scientists and policy makers~~ The results of this study can provide forest managers with
basic reference on the carbon sequestration potential of different Chinese subtropical forests. Moreover,
investigating the dynamics of GPP and their dominant driving factors in the study area is crucial for
decision-makers to adjust and optimize forest management policies promptly, so as to ensure that forests
145 can provide the best ecological services for humans.

2. Materials and methods

2.1 Study area description

In this study, we focused on China's subtropical forests which account for approximately 64%
(~1.25 × 10⁶ km²) of the total forested area in China, and the boundary of the subtropical region was
150 derived from the Resource and Environment Science and Data Center of China (He et al., 2021a; He et
al., 2019), which covers a latitudinal range of 21.33–33.91°N and a longitudinal range of 91.39–122.49°E

and has a typical subtropical monsoon climate. The mean annual temperature in the study area is about 15.5°C, and it normally increases from the northwest toward the southeast.~~The average annual temperature is about 15.5°C and the~~The mean annual precipitation ranges from 800 mm in the north to more than 2000 mm in the south, with 80% of precipitation concentrated in the growing season. The main forest types in the subtropical region of China include the evergreen broadleaved forest (EBF), evergreen needle-leaved forest (ENF), deciduous broadleaved forest (DBF), and mixed forest (MXF) (Fig.1). There are three operating flux towers in the area: Qianyanzhou (QYZ), Dinghushan (DHS), and Ailaoshan (ALS). A more detailed description of these flux tower sites can be found in Table S1.

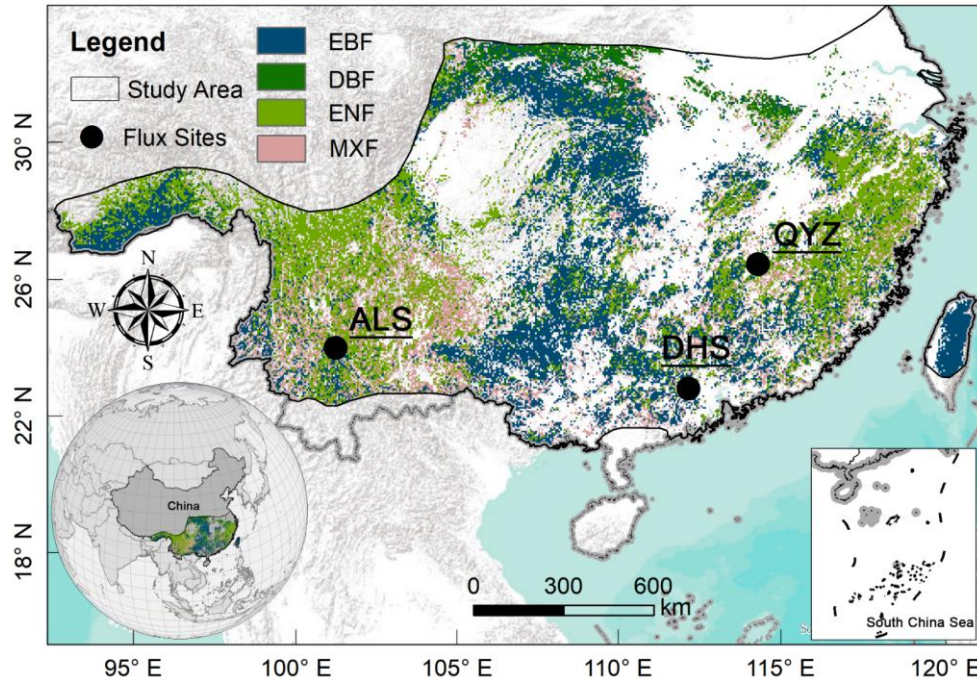


Figure 1 Location of the study area and 3 flux sites. The forest cover map (2018) shown here was derived from the European Space Agency land cover data (ESA CCI-LC). The forest types of ALS and DHS are EBF, and the forest type of QYZ is ENF.

2.2 Model description

In this study, we used the BEPS model to simulate the subtropical forest GPP and NEP (i.e., net ecosystem productivity) with a resolution of 0.05°. The BEPS is a process-based model driven by the remotely sensed leaf area index (LAI), land cover types, soil ~~data~~, and meteorological data. Recently, the BEPS model was used to simulate the terrestrial ecosystem carbon and water fluxes over different regions, such as the globe (Chen et al., 2019b; Chen et al., 2012), North America (Sprintsin et al., 2012; Xie et al., 2018), Europe (Wang et al., 2003), East Asia (Matsushita and Tamura, 2002), as well as the whole or southern China (Liu et al., 2018; Liu et al., 2014; Peng et al., 2021). A more detailed description of the original BEPS can be found in Supplementary section Text S1 and previous studies (Chen et al., 2019b; Chen et al., 1999; Ju et al., 2006; Liu et al., 1999; Liu et al., 1997). In BEPS, ~~the~~ daily GPP ($\text{gC m}^{-2}\text{day}^{-1}$) is calculated as (Chen et al., 1999):

$$\text{GPP} = \text{GPP}_{\text{sun}}\text{LAI}_{\text{sun}} + \text{GPP}_{\text{shade}}\text{LAI}_{\text{shade}} \quad (1)$$

where GPP_{sun} ($\text{gC m}^{-2}\text{day}^{-1}$) and $\text{GPP}_{\text{shade}}$ ($\text{gC m}^{-2}\text{day}^{-1}$) denote the GPP per unit area of sunlit and

shaded leaves; LAI_{sun} ($m^2 m^{-2}$) and LAI_{shade} ($m^2 m^{-2}$) respectively represent the LAI of sunlit and shaded leaves. LAI_{sun} and LAI_{shade} depend on the mean solar zenith angle (θ , unitless):

$$LAI_{sun} = 2\cos\theta \times (1 - \exp(-0.5\Omega LAI/\cos\theta)) \quad (2)$$

$$LAI_{shade} = LAI - LAI_{sun} \quad (3)$$

where LAI is the total canopy leaf area index ($m^2 m^{-2}$) and Ω is the clumping index (unitless).

In the BEPS model, the maximum carboxylation rate V_{cmax} ($\mu mol m^{-2} s^{-1}$) is one of the important and sensitive parameters to influence the ~~photosynthesis-photosynthetic~~ rate of plants and estimate the carbon fluxes (Croft et al., 2017; Luo et al., 2019). V_{cmax} mainly depends on V_{cmax25} and air temperature (T_a , °C) in BEPS model, see supplementary section Text S1 (Eq. S4). Generally, V_{cmax25} is a commonly defined constant among different plant functional types (PFTs) in the model. However, V_{cmax25} actually has large spatial variations (Table S2) due to the changes of species composition, soil properties, and climates within the same PFT, even observations showed a 2-3 fold variation in V_{cmax25} for the same PFT (Chen et al., 2022b). As a result, using a PFT with fixed V_{cmax25} in the model may distort the spatial distribution of the GPP simulation (Chen et al., 2022b). Therefore, in this study, we introduced a spatial variation of V_{cmax25} derived from remote sensing data to replace the constant V_{cmax25} in the original BEPS model. The other parameters, including the clumping index, maximum stomatal conductance, specific leaf area, respiration coefficient for leaf, stem, coarse root, and fine root, Q10 for leaf, stem, and root, etc., used in the BEPS model for each plant functional type can be found in Liu et al. (2018), which were specially parameterized for ~~the simulation-simulating of~~ the carbon fluxes of terrestrial ecosystems in China based on the flux tower observations (Liu et al., 2013a; Liu et al., 2016; Liu et al., 2013b) and the published literature (Feng et al., 2007; Liu et al., 2015; Zhang et al., 2012).

2.3 Data and processing

(1) Flux tower data

To evaluate the models' performance, we acquired the daily eddy covariance (EC)-derived GPP and NEP (net ecosystem productivity) from three flux tower sites over the study area (Fig. 1), which was available from the ChinaFLUX network (Yu et al., 2006). The ChinaFLUX has undergone strict data quality control, including coordinate rotation, Webb-Pearman-Lenuing (WPL) correction, and nighttime flux correction, gap filling, and flux partitioning. For instance, the nighttime CO₂ flux data under low atmospheric turbulence conditions were screened using site-specific thresholds of friction velocity (u^*), which was identified following Reichstein et al. (2005) For instance, the nighttime CO₂ flux correction mainly includes removing outliers when there is precipitation, CO₂ concentration exceeds the instrument's measurement range, insufficient turbulence (e.g., the threshold of $u^* < 0.2 m s^{-1}$ was used for the QYZ and ALS stations, while the threshold of $u^* < 0.05 m s^{-1}$ was used for the DHS station), and less than 15,000 valid samples, and the NEE was also partitioned into GEP and ER with the method of Reichstein et al. (2005).

(2) Remote sensing data

LAI. The Global Land Surface Satellite (GLASS) LAI product during 2001-2018 was obtained from the University of Maryland. This data was generated using the general regression neural networks

(GRNNs) with a spatiotemporal resolution of 0.05° and 8-day (Xiao et al., 2016). The daily LAI at 0.05° resolution was obtained by linear interpolation of the 8-day GLASS LAI, which was used to drive the BEPS model (Wang et al., 2022). The GLASS LAI was used in this study because of its higher accuracy in China's forests compared to other satellite LAI products, such as the GEOVI LAI, etc. (Liu et al., 2018; Xie et al., 2019). For example, Liu et al. (2018) estimated the accuracy of different satellite-derived LAI products for the simulation of carbon and water fluxes in China's forests based on the BEPS model, and proved that GLASS LAI showed higher accuracy in simulating forest GPP than other LAI products (e.g., FSGOM LAI and MODIS LAI). The consistent conclusions also have been reported in other studies (Chen et al., 2021a; Jiang et al., 2017; Xie et al., 2019). Therefore, it was reasonable to use GLASS LAI as input to model subtropical forest GPP in this study.

Satellite-derived $V_{\text{cmax}25}$ products. We obtained the spatial variation of satellite-derived $V_{\text{cmax}25}$ products from the National Ecosystem Science Data Center, National Science & Technology Infrastructure of China, available spanning from 2000 to 2019, with a spatiotemporal resolution of 500m and 8-day. We used an average yearly~~the annual mean~~ $V_{\text{cmax}25}$ for each pixel that varied from year to year (2001-2018), and it was further resampled to $0.05^\circ \times 0.05^\circ$ for driving the model. The $V_{\text{cmax}25}$ product was produced by satellite-derived leaf chlorophyll content (LCC) (Xu et al., 2022) and a semi-mechanistic model (Lu et al., 2022). ~~It has been shown to be robust enough to reduce uncertainty in BEPS model simulations. It has been shown that this can effectively reduce the uncertainty in the simulations of the BEPS model.~~ (Lu et al., 2022; Lu et al., 2020; Wang et al., 2020b). More mechanisms for deriving $V_{\text{cmax}25}$ from remote sensing data are available in Lu et al. (2022), Luo et al. (2018), and Xu et al. (2022).

Published GPP products. To better estimate the model performance of the BEPS model, we also used five global GPP products generated by different methods to compare with our simulated GPP, which were further aggregated into $0.05^\circ \times 0.05^\circ$ for comparison. The five published GPP products include (a) the MODIS GPP (MOD17A2H Version 6) (Running et al., 2015), (b) the EC-LUE GPP generated by a revised light use efficiency model (Zheng et al., 2020), (c) the NIRv GPP produced by near-infrared reflectance (NIR_v) and machine learning method (Wang et al., 2021b), (d) the VPM GPP produced by the Vegetation Photosynthesis Model (VPM) (Zhang et al., 2017), and (e) another published BEPS GPP product (hereinafter referred to as BEPS_g GPP), which was also generated by the BEPS model but with independent driving data and globally calibrated parameters (Chen et al., 2019b; He et al., 2021b). See Table S3 for more details on the five GPP products.

(3) Climate data

We obtained the daily meteorological data including the temperature, precipitation, relative humidity, and downward solar radiation from the Climate Meteorological Forcing Dataset (CMFD) (He et al., 2020), and used ~~it~~them to drive the BEPS model. The CMFD is a high spatial (about 0.1°) and temporal (e.g., hourly and daily) resolution reanalysis product and covers the period of 1979-2018, which has been evaluated against the in-situ meteorological data (He et al., 2020) and were widely used in previous studies (Huang et al., 2021; Wang et al., 2020a; Yang et al., 2017a). To ensure consistency with the resolution of ~~the other~~ drivers~~driving data~~, the CMFD was also resampled to 0.05° based on the

250 bilinear interpolation method.

(4) Land cover data

The annual land cover data sets from the European Space Agency (ESA) were used for simulations (ESA, 2017). The ESA CCI land cover data has a resolution of 300 meters, spanning the 1992-present period. The overall global accuracy of CCI land cover data is nearly 75.4%, with higher accuracy for forests (ESA, 2017). In this study, the original CCI land cover data were first aggregated into $0.05^\circ \times 0.05^\circ$ by using the CCI LC user tool. Considering the CCI land cover data composed of 37 ~~original classes~~ original vegetation classes, we referred to (Tagesson et al., 2020) to reclassify the CCI land cover data into 9 classes, including the evergreen broadleaved forest (EBF), evergreen needleleaved forest (ENF), deciduous broadleaved forest (DBF), and mixed forest (MF), cropland (CRO), grassland (GRA), shrubland (SHR), urban (URB), and barren land (BAR).

(5) Soil and atmospheric CO₂ data

The available water capacity (AWC) data with a spatial resolution of 0.05° was extracted from the re-gridded Harmonized World Soil Database (RHWSO) v1.2 (FAO, 2012; Wieder et al., 2014) and used to drive the model in this study. We obtained the annual mean atmospheric CO₂ concentration data (2001-2018) from the Hawaiian Mauna Loa observatory.

2.4 Experiment design

To understand the individual and combined effects of forest cover change, LAI ~~vegetation structure change~~, CO₂ fertilization, and climate change on annual subtropical forest GPP variations during 2001-2018, we designed five groups of simulations in this study (Table 1). First, in scenario S_{baseline}, the model was run based on all the dynamic inputs during 2001-2018, including the dynamic land cover, LAI, CO₂, and all climate variables. In scenario S₁, we fixed the land cover in 2001 and allowed all other driven data to vary from 2001 to 2018. ~~It should be noted that in this scenario, land cover change may lead to changes in LAI and thus forest GPP, such as the conversion of forest to non-forest or vice versa, however, the direct cause of LAI change in this scenario is actually due to forest cover change, thus in the present study we set this part of GPP change as the contribution of land cover change (Chen et al., 2021a).~~ In scenario S₂, we conducted four different simulations to investigate how the key climatic factors (S_{2.1}: precipitation; S_{2.2}: temperature; S_{2.3}: solar radiation) and all climate change (S_{2.4}) influence the subtropical forest GPP. We individually fixed the precipitation, temperature, solar radiation, and all climatic factors in the year 2001, while allowed all other factors (i.e., land cover, LAI, and CO₂) to change over time. In scenario S₃, the LAI was fixed at the level of 2001 and other factors were changed over time. In scenario S₄, we fixed CO₂ concentration (371.31 ppm) in 2001, with other drivers being dynamics. Finally, the difference between S_{baseline} and different scenarios ~~was~~ were calculated for estimating the effect of different drivers on subtropical forest GPP changes.

Table 1 Design of the scenarios for unravelling the effect of forest cover change, LAI ~~vegetation structure change~~, CO₂ fertilization, and climate change on subtropical forest GPP variations.

Scenarios	Land cover	LAI	Climate	Atmospheric CO ₂	Purpose
-----------	------------	-----	---------	-----------------------------	---------

S_{baseline}	Dynamic	Dynamic	Dynamic	Dynamic	Estimating actual dynamics of GPP	
S_1	Fixed in 2001	Dynamic	Dynamic	Dynamic	Estimating the effect of forest cover change on GPP	
S_2	$S_{2.1}$	Dynamic	Dynamic	Fixed in 2001	Dynamic	Estimating the effect of precipitation on GPP
	$S_{2.2}$	Dynamic	Dynamic	Fixed in 2001	Dynamic	Estimating the effect of temperature on GPP
	$S_{2.3}$	Dynamic	Dynamic	Fixed in 2001	Dynamic	Estimating the effect of radiation on GPP
	$S_{2.4}$	Dynamic	Dynamic	Fixed in 2001	Dynamic	Estimating the effect of climate change on GPP
S_3	Dynamic	Fixed in 2001	Dynamic	Dynamic	Estimating the effect of vegetation structural change LAI on GPP	
S_4	Dynamic	Dynamic	Dynamic	Fixed in 2001	Estimating the effect of CO ₂ fertilization on GPP	

2.5 Statistical analysis

Three statistical metrics were used to assess the performance of the BEPS model in the simulation of GPP and NEP. These metrics include the coefficient of determination (R^2), the root mean square error (RMSE), and the mean bias error (MBE).

The average values of 3×3 pixels centered around the flux sites (provided that these grid pixels have the same land cover type) were used to validate the predicted GPP and NEP (Peng et al., 2021; Wang et al., 2022). In addition, the linear regression analysis was used to detect the long-term trend of the differences between the real and control experiments, which ~~was~~ were considered as the impact of the controlled variable on the GPP changes.

Moreover, the spatial correlation was adopted in this study to compare the spatial consistency of our simulated GPP with other GPP products. The spatial correlation was calculated pixel by pixel at the annual scale. First, two GPP time series for a certain pixel were obtained in the same period, and then the correlation between the two GPPs was calculated. By analogy, the spatial distribution of the correlation coefficients can be achieved.

3. Results

3.1 Model performance

We first compared the simulated daily GPP with the flux-site GPP (Fig. 2). The overall accuracy of GPP simulated by the BEPS model agreed well with measurements from the three flux sites (ALS: $R^2 = 0.58$, RMSE = $1.57 \text{ gC m}^{-2} \text{ day}^{-1}$, and MBE = $0.03 \text{ gC m}^{-2} \text{ day}^{-1}$; DHS: $R^2 = 0.44$, RMSE = $1.17 \text{ gC m}^{-2} \text{ day}^{-1}$, and MBE = $0.25 \text{ gC m}^{-2} \text{ day}^{-1}$; QYZ: $R^2 = 0.77$, RMSE = $1.36 \text{ gC m}^{-2} \text{ day}^{-1}$, and MBE = $0.05 \text{ gC m}^{-2} \text{ day}^{-1}$) (Fig. 2a-c). The BEPS model also showed good performance in simulating daily GPP each year (Table S4, Fig. S1-S3). For example, the R^2 ranged between 0.50 and 0.72 for ALS (2009-2013), ~~ranged~~ between 0.43 and 0.65 for DHS (~~2003~~2003-2010), and ~~ranged~~ between 0.70 and 0.85 for QYZ (~~2003~~2003-2010). Simulated GPP also captured both the absolute values and the inter-annual variability of observed annual GPP ~~for~~ in the three flux sites (Fig. 2d-f). Compared with the yearly measured GPP, the overall accuracy (R^2) of GPP simulated by the BEPS model was 0.89 (ALS), 0.53 (DHS), and 0.73

(QYZ), respectively (Fig. 2 d-f). We further examined the BEPS model in simulating daily NEP, which also showed the BEPS model agreed reasonably well with measured daily NEP (Table S5, Fig. S4-S6). The overall accuracy (R^2) of simulated daily NEP was 0.25 (ALS), 0.35 (DHS), and 0.42 (QYZ), respectively (Table S5). However, the simulation accuracy of NEP was generally lower than that of GPP (Table S4-S5). In this study, we used the NEP for testing the model performance, because NEP (i.e., -NEE (net ecosystem exchange)) is a direct measurement of carbon fluxes between the atmosphere and ecosystems. Therefore, we not only used the observed GPP from the flux sites to validate our model, but also the NEP. The validation of model performance based on measured NEP was relatively lower than that of GPP. One cause is that the simulation of NEP in the model is influenced not only by the accuracy of simulated GPP, but also by the accuracy of simulated heterotrophic respiration (R_h) and autotrophic respiration (R_a).

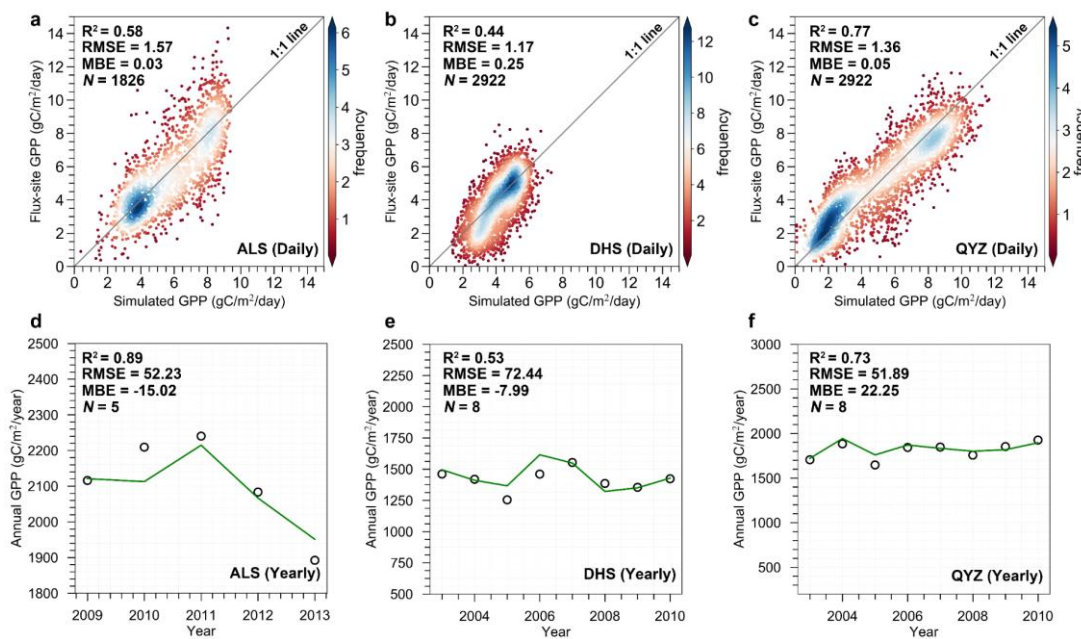


Figure 2 Comparison of simulated GPP with measured GPP from three flux tower stations at daily (a-c) and annual (d-f) scales. The green lines and dark circles represent the simulated GPP and observed GPP, respectively.

At the regional level, the BEPS model captured well the spatial gradient in GPP when compared with the other GPP products (Fig. [3S7](#)). The mean R^2 values between our simulated GPP and NIRv GPP, EC-LUE GPP, MODIS GPP, BEPS GPP, and VPM GPP were 0.52, 0.67, 0.41, 0.54, and 0.41, respectively (see Fig. [S7FS8f](#)). Especially, the simulated GPP was well consistent with the spatial pattern of the EC-LUE GPP (Fig. [S8bS7](#)). In nearly 67% and 34% of forest areas, the R^2 was higher than 0.6 and 0.8, respectively. Besides, we compared the multi-year mean of annual total GPP in our study with the other five GPP products among the entire forest and different forest types (Fig. [S9S8](#)). The multi-year mean of annual total GPP for the entire forest area in our study is $2.23 \pm 0.14 \text{ PgC year}^{-1}$, which closing to the magnitudes of the three GPP products which failed in the range of the five GPP products (i.e., another BEPS_g GPP product: $2.54 \pm 0.16 \text{ PgC year}^{-1}$; MODIS GPP: $2.10 \pm 0.07 \text{ PgC year}^{-1}$; VPM GPP: $2.05 \pm 0.10 \text{ PgC year}^{-1}$) and the mean of the five GPP products ($2.07 \pm 0.11 \text{ PgC year}^{-1}$).

340 respectively-(Fig. S9S8). Meanwhile, for the entire and different forests, the annual GPP of this study and other GPP products also showed a similar increasing trend (Fig. S8fS9f-8j9j). For example, such as the trend of the entire forests DBF and MXF in this study ($0.026 \text{ PgC year}^{-1}$, $p < 0.001$) was closed to the BEPS-VPM GPP ($0.028 \text{ PgC year}^{-1}$, $p < 0.001$) and the VPM-EC-LUE GPP ($0.017 \text{ PgC year}^{-1}$, $p < 0.001$) (Fig. S8fS9h, Fig. S9j). Overall, all the evaluations indicated that the performance of the BEPS model was reasonably well in simulating GPP in the study area. Although our simulated GPP is slightly higher for the entire subtropical forests, EBF and ENF than other GPP products, it is very close to other GPP products for specific forest types such as DBF and MXF (Fig. S9). Similarly, these commonly used GPP products also have large differences when compared to each other (Fig. S9). These results indicate that there is still a large discrepancy in modelling GPP to date, due to many differences in model structure, parameterization, and driving data. For example, the MODIS GPP was mainly generated by the Terra/Aqua satellite observations, while the newly released NIRv GPP was produced by near-infrared reflectance (i.e., the AVHRR reflectance from LTDR (Land Long Term Data Record v4) product). Thus, the data sources derived from divergent satellite observations may result in the differences between the two GPPs. Additionally, the EC-LUE GPP, VPM GPP, and the BEPS_g GPP are all model outputs, where EC-LUE GPP and VPM GPP are simulated by different light use efficiency (LUE) models, respectively, and the BEPS_g GPP is produced by a process model. However, current LUE-based models do not completely integrate other key environmental regulations to vegetation productivity, such as the effect of atmospheric CO₂ concentration. Thus, the underestimation in other GPP products is possibly due to failure to assess the CO₂ fertilizer effects, because almost no apparent response to the rising atmospheric CO₂ concentration in the LUE models leads to an underestimated trend. In our study, the GPP was estimated by a process-based model (i.e., BEPS) that considers the CO₂ fertilization effect, which may lead to a higher GPP when compared to other GPP products.

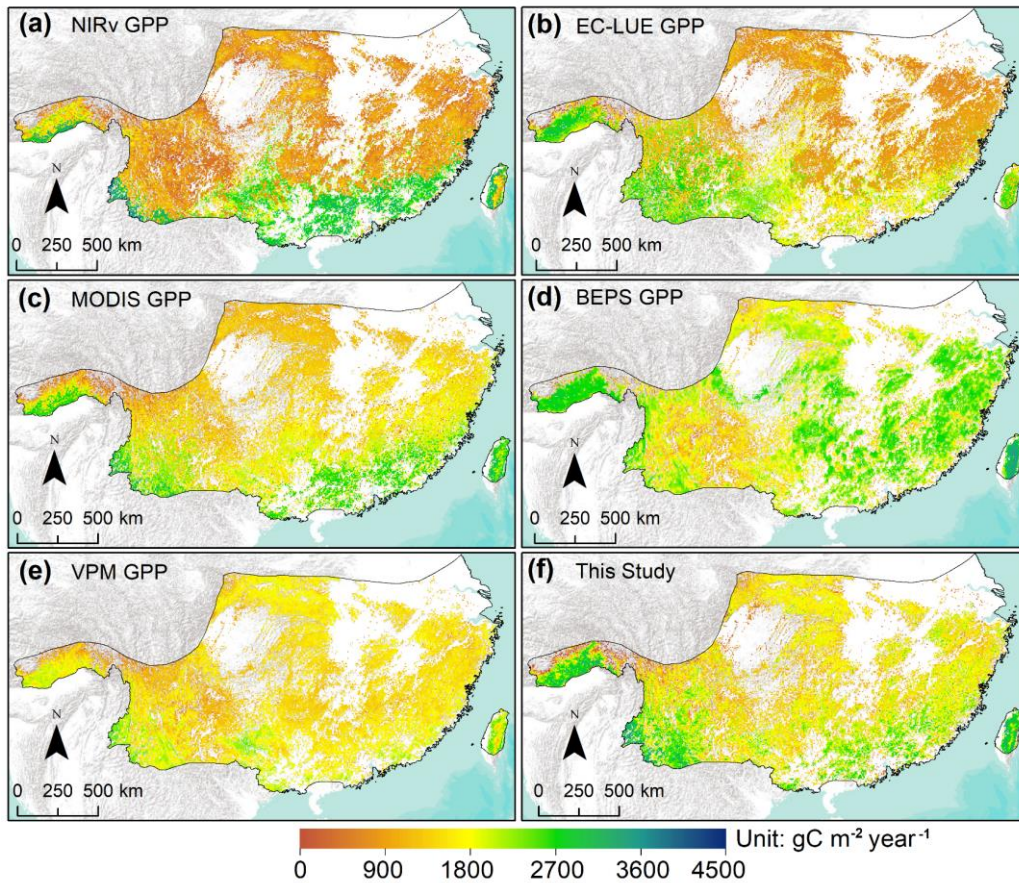
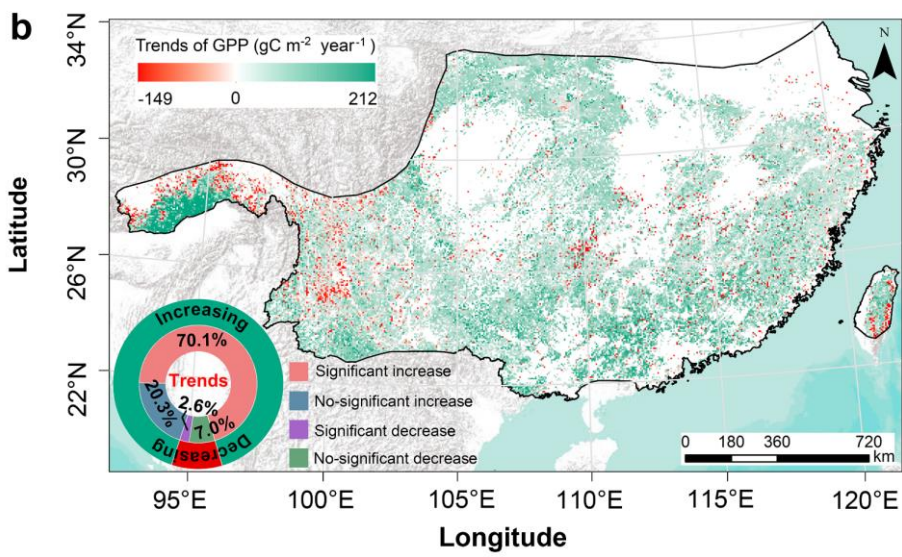
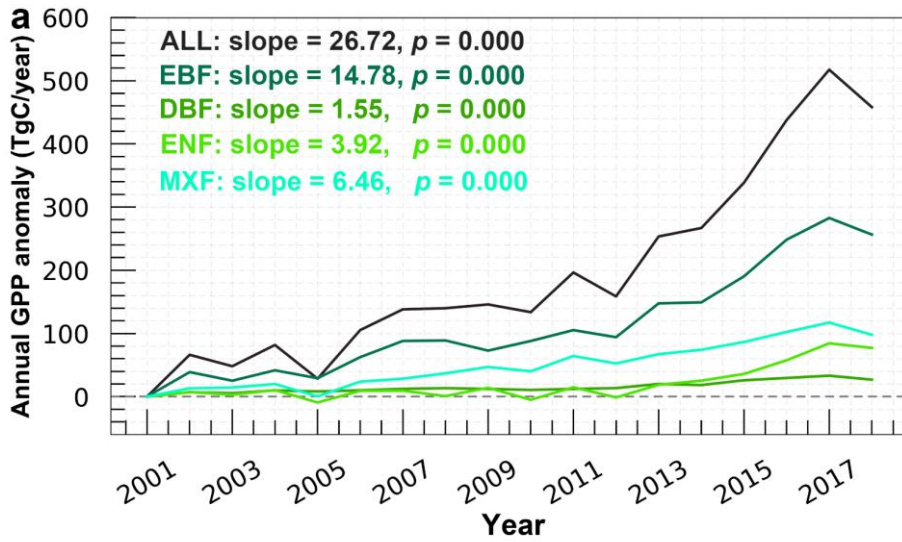


Figure 3 Comparison of the spatial distribution of the mean annual GPP. (a) NIRv GPP, (b) EC-LUE GPP, (c) MODIS GPP, (d) another published BEPS GPP, and (f) our simulated GPP. All the maps were calculated over the 2001–2018 period, except for VPM GPP which is only available from 2001 to 2016.

3.2 Spatiotemporal variations of the subtropical forest GPP

The simulated actual GPP showed a significant increasing trend ($20.67 \text{ gC/m}^2/\text{year}$ to $26.72 \text{ TgC year}^{-1}$, $p = 0.000$) during 2001–2018 over the entire subtropical forests due to the interactive effect of different drivers (Fig. 4a3a). Among the four forest types, the EBF showed the largest significantly increasing trend ($28.24 \text{ gC/m}^2/\text{year}$ to $14.78 \text{ TgC year}^{-1}$, $p = 0.000$), followed by DBF ($20.68 \text{ gC/m}^2/\text{year}$ to $1.55 \text{ TgC year}^{-1}$, $p = 0.000$), the MXF ($16.12 \text{ gC/m}^2/\text{year}$ to $6.46 \text{ TgC year}^{-1}$, $p = 0.000$), and ENF ($15.20 \text{ gC/m}^2/\text{year}$ to $3.92 \text{ TgC year}^{-1}$, $p = 0.000$). Spatially, 90.4% of forested land in the study area showed an increasing trend in GPP, while 9.6% of forested land exhibited a decreasing trend in GPP. Spatially, 90.4% and 9.6% of the forest GPP showed increased and decreased, respectively (Fig. 3b). Among them, the areas with the significantly increased and decreased GPP respectively accounted for 70.1% and 2.6% of the total entire subtropical forest area, respectively (Fig. 3b).



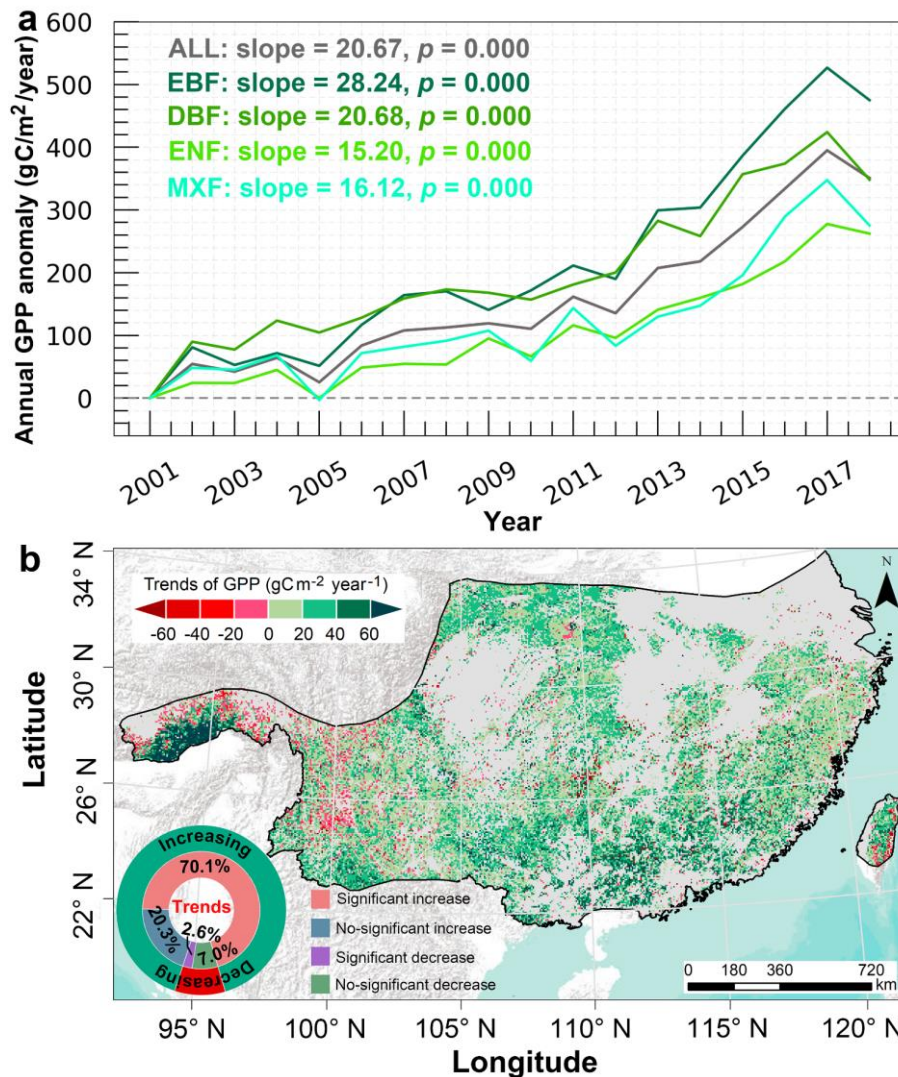


Figure 4.3 (a) Temporal variations of the annual subtropical forest GPP anomaly during 2001-2018, and the annual GPP anomaly is calculated relative to the base year of 2001; (b) Spatial distribution of the annual trends in actual GPP.

3.3 Disentangling the effects of driving factors on subtropical forest GPP changes

3.3.1 Impacts of forest cover changed different driving factors on subtropical forest GPP changes

We investigated the area of gains or losses for different subtropical forest types between 2001 and 2018 using the ESA CCI land cover data (Fig. S10). We found that FCC increased the entire subtropical forest GPP at a rate of 0.52 gC/m²/year ($p = 0.000$) (Fig. 4a), and the increase mainly driven by EBF GPP (0.39 gC/m²/year, $p = 0.011$) and MXF GPP (1.14 gC/m²/year, $p = 0.000$). However, the FCC had a negative effect on the DBF GPP and ENF GPP variations at the rate of -0.06 gC/m²/year ($p = 0.632$) and -0.19 gC/m²/year ($p = 0.002$), respectively. Spatially, 92.2% of the total GPP were relatively stable, and only 7.8% of GPP exhibited an increase or decrease under the effect of FCC (Fig. 4b). Among them, 3.9% of the GPP increased significantly and the increased were mainly located in the western region (e.g., the south slope of the Qinling mountains, the southwest karst region), while 2.6% of the GPP was significantly reduced in the eastern regions where the ENF is dominated (Fig. 4b).

Based on the ESA CCI land cover data between 2001 and 2018, it showed that the EBF and MXF

395 had a net increase of 17,340 km² and 11,660 km², respectively, while the ENF showed a negative net
 net change (-16,580 km²) and the DBF was almost unchanged between 2001 and 2018 (Fig. 5). As a whole,
 the total forest area in our study area showed a net increase change of 12,800 km² (Fig. 5a). We found
 that FCC positively affected the entire forest GPP at a rate of 1.35 TgC year⁻¹ ($p = 0.000$) (Fig. 5b),
 mainly driven by EBF GPP (1.17 TgC year⁻¹, $p = 0.001$) and MXF GPP (2.15 TgC year⁻¹, $p = 0.000$).
 400 However, the FCC had a negative effect on the DBF GPP and ENF GPP variations at the rate of -0.05
 TgC year⁻¹ ($p = 0.195$) and -1.92 TgC year⁻¹ ($p = 0.000$), respectively. Spatially, 92.2% of the total forest
 GPP showed a stable state, and only 7.8% of GPP exhibited an increase or decrease under the effect of
 FCC (Fig. 5c). Among them, 3.9% of the forest GPP increased significantly, mainly located in the
 western region (e.g., the south slope of the Qinling mountains, the southwest karst region), while 2.6%
 405 of the forest GPP was significantly reduced in the eastern regions, which belong to the ENF (Fig. 5).

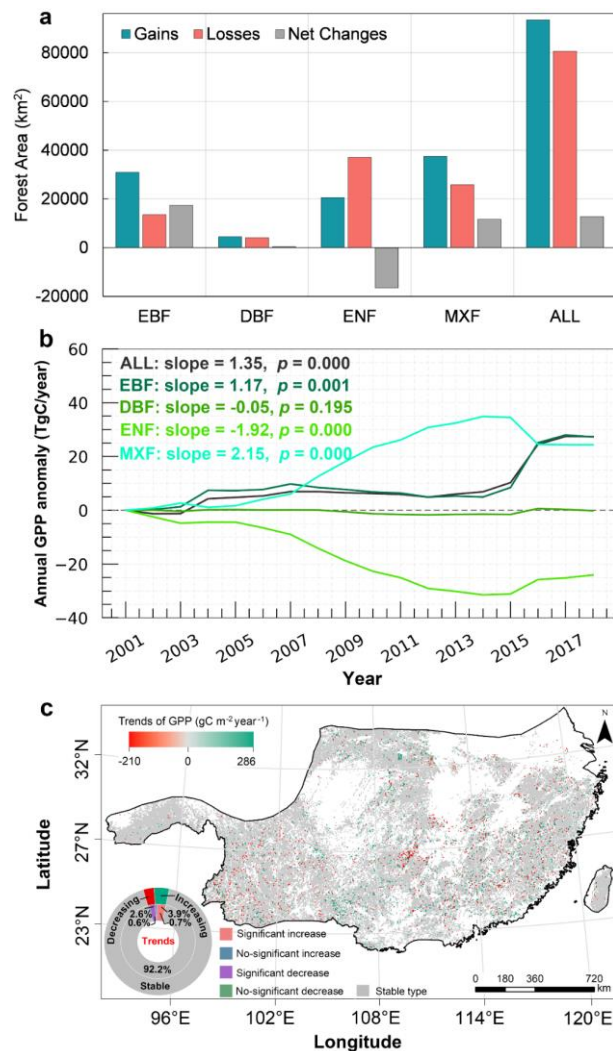


Figure 5 (a) Changes in forest areas between 2001 and 2018. (b) Temporal variation of the effect of forest cover change on annual forest GPP changes. (c) Spatial distribution of the impacts of forest cover change on GPP.

3.3.2 Impacts of climate change on forest GPP changes

The annual total precipitation and annual mean temperature over the entire forest region and different forest areas showed an increasing trend, while the annual total radiation displayed a decreasing

trend for the entire forest region and different forest areas (Fig. S11). The individual effect of precipitation, temperature, and solar radiation on subtropical forest GPP was first investigated in Fig S12, and their combined effects on GPP changes were shown in Fig. 4c-d. The results showed that climate change increased the GPP across the entire forest area (0.92 gC/m²/year, $p = 0.080$), especially a significant increase in the EBF (3.83 gC/m²/year, $p = 0.000$) and DBF (2.49 gC/m²/year, $p = 0.003$), while the climate change decreased the GPP of ENF (-1.22 gC/m²/year, $p = 0.016$) and MXF (-1.23 gC/m²/year, $p = 0.075$) (Fig. 4c). Spatially, 10.3% and 19.1% of the study area exhibited a significant upward trend and downward trend (Fig. 4d), respectively, due to the effect of climate change. Overall, increase in GPP induced by precipitation, temperature, and solar radiation change heavily erases their negative effects on GPP, making climate change contribute to GPP increase in the whole study area. Simulation results showed that an increase in precipitation induced the GPP enhancement at the rate of 0.26 TgC year⁻¹ ($p = 0.541$) for all the forest types together (Fig. 6a). The negative effect of precipitation on ENF GPP (-0.02 TgC year⁻¹, $p = 0.618$) and MXF GPP (-0.14 TgC year⁻¹, $p = 0.137$) was mainly offset by EBF GPP (0.33 TgC year⁻¹, $p = 0.304$) and DBF GPP (0.09 TgC year⁻¹, $p = 0.013$) enhancements (Fig. 6a). Spatially, the positive effect of precipitation on GPP changes accounted for most parts of the total area (87.5%), of which 3.1% showed a significant ($p < 0.05$) increase, mainly located in the west and north, which was consistent with the trends in the spatial distribution of precipitation (Fig. S9b). Precipitation also caused a small part of GPP (12.5%) decrease, and there is almost no significant decrease trend (Fig. 6b). Changes in temperature slightly increased the GPP across all forest types (Fig. 6c), but it showed great spatial variations (Fig. 6d). The significantly negative effect of temperature on GPP (13.3%) was mainly distributed in the south and west, while the significantly positive effect of temperature on GPP (8.9%) was mainly located in the western mountainous areas (Fig. 6d). Decreasing solar radiation (Fig. 6e) led to the negative impact of all the forest area (-1.13 TgC year⁻¹, $p = 0.162$) as well as different forest types (EBF: -0.35 TgC year⁻¹, $p = 0.263$; DBF: -0.05 TgC year⁻¹, $p = 0.442$; ENF: -0.51 TgC year⁻¹, $p = 0.126$; MXF: -0.22 TgC year⁻¹, $p = 0.201$). The decrease in solar radiation caused a significant decrease in GPP of 10.1% ($p < 0.05$) (Figure 6f). A small portion of the study areas exhibited GPP enhancement under the influence of solar radiation, but it was hardly significant (3.3%).

Ultimately, the combined and interactive effects of climate change resulted in an increase in GPP across the entire forest area (1.11 TgC year⁻¹, $p = 0.080$), especially a significant increase in the EBF (1.76 TgC year⁻¹, $p = 0.000$) and DBF (0.18 TgC year⁻¹, $p = 0.003$), while the climate change led to the decrease in ENF (-0.53 TgC year⁻¹, $p = 0.016$) and MXF (-0.29 TgC year⁻¹, $p = 0.792$) (Fig. 6g). Nearly 41.8% of the study area exhibited an upward trend due to the effect of climate change, mainly distributed in the west and the north (Fig. 6f), of which 10.3% showed a significant ($p < 0.05$) increase. On the contrary, 58.2% of the study area (a significant area accounted for 6.4%) showed a decreasing trend, mainly located in the east, central, and southwest (Fig. 6f). Overall, the increase in GPP induced by precipitation, temperature, and solar radiation can erase their negative effects on GPP, making climate change contribute to GPP increase in the whole study area. Although all the main climatic factors did not change significantly during the study period, their combined effects would have a significant impact on different subtropical forest GPP changes (Fig. 6g and 6h), suggesting that different subtropical forest GPP has a different sensitivity to climate change.

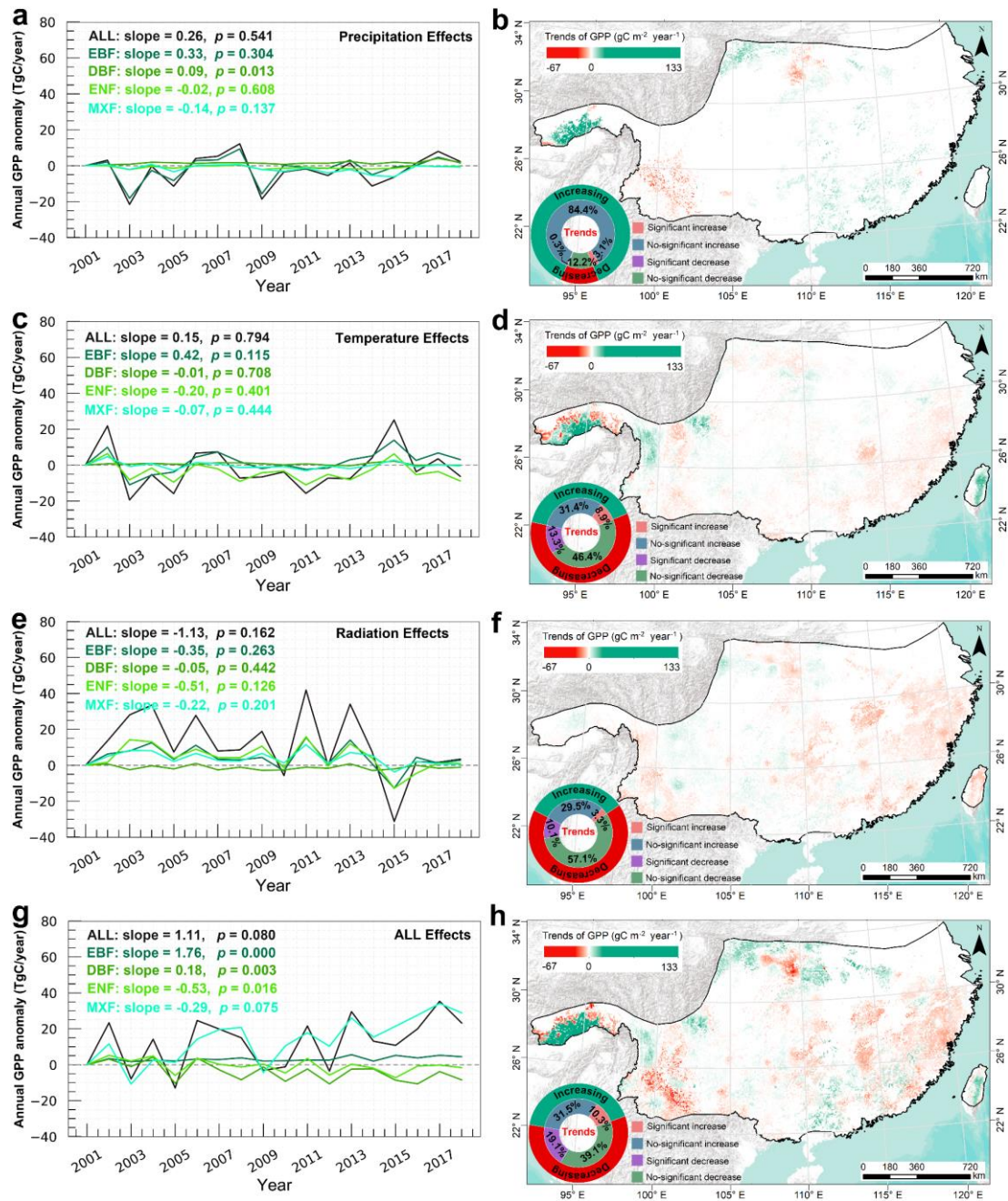


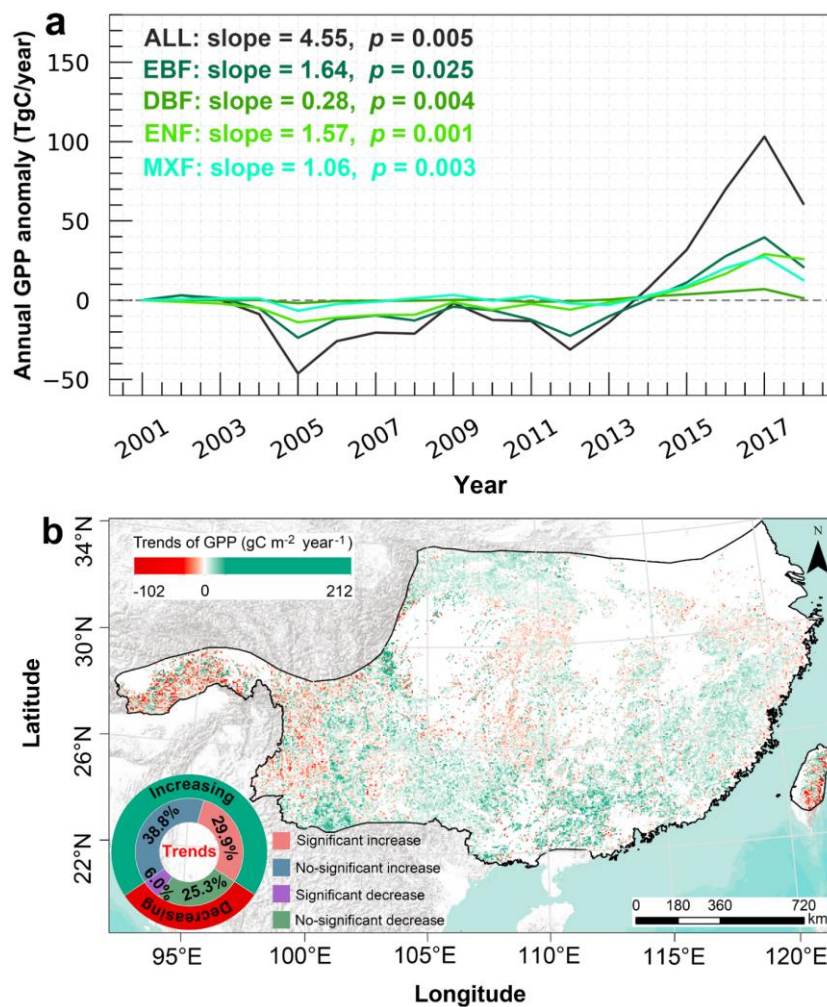
Figure 6 Temporal variation of the effects of precipitation (a), temperature (c), solar radiation (e), and all climate changes (g) on annual GPP trends. Spatial distribution of the impacts of precipitation (b), temperature (d), solar radiation (f), and all climate changes (h) on subtropical forest GPP.

3.3.3 Impacts of LAI change on forest GPP changes

The LAI of entire and different forests showed significant upward trends during the study period (Fig. S13). The simulations showed that LAI exerted a significant positive effect of $3.79 \text{ gC/m}^2/\text{year}$ ($p = 0.004$) in the entire forest region (Fig. 4e), confirming the positive role of LAI in subtropical forest GPP variations. There was significant spatial heterogeneity in the effect of LAI on GPP changes (Fig. 4f). A significant ($p < 0.05$) positive effect of LAI on GPP was observed over 29.9% of the study area and these areas are mainly located in the south and north (Fig. 4f). The areas with a significant decreasing trend ($p < 0.05$) accounted for 6.0% and are mainly distributed in the western and central parts of the

465 study area (Fig. 4f). There are more positive changes in GPP due to the effect of LAI that heavily offsets
 470 the negative changes in GPP, ultimately making LAI the main factor in GPP increases throughout China's
 subtropical forests.

The LAI of entire and different forests showed significant upward trends during the study period
 (Fig. S10). The simulations showed that the VSC exerted a significant positive effect of 4.55 TgC year⁻¹
 (p = 0.005) for the entire forest region (Fig. 7a), confirming the positive role of VSC in forest GPP
 variations. Especially, the positive effect of VSC on EBF (1.64 TgC year⁻¹, p = 0.025) contributed the
 most to the GPP increment (Fig. 7a). There was significant spatial heterogeneity in the effect of VSC on
 GPP changes (Fig. 7b). A positive effect of VSC on GPP was observed over 68.7% of all forest types
 together, where GPP increased significantly (p < 0.05) in 29.9% of the total study area. Most of the
 475 significantly increasing areas were located in the south and north (Fig. 7b). The areas with a significant
 decreasing trend (p < 0.05) accounted for 6.0%, and they were mainly distributed in the western and
 central parts of the study area (Fig. 7b). Overall, the results showed that most GPP increases in China's
 subtropical forests due to the increase of LAI, which also offset the negative effects of VSC on GPP, thus
 allowing VSC to play a key driving factor in promoting GPP increases throughout the forest area.



480 **Figure 7** Temporal variation (a) and spatial distribution (b) of the effects of VSC on forest GPP.

3.3.4 Impacts of CO₂ fertilization on forest GPP changes

The annual mean CO₂ concentration increased from 371.3 ppm to 408.7 ppm during 2001-2018 (Fig. S14), which led to a significant increase of all subtropical forest GPP at the rate of 6.84 gC/m²/year ($p = 0.000$) (Fig. 4g). The significantly positive effects of CO₂ fertilization on EBF GPP (6.91 gC/m²/year, $p = 0.000$) and ENF GPP (7.02 gC/m²/year, $p = 0.000$) was higher than that of DBF GPP (5.93 gC/m²/year, $p = 0.000$) and MXF GPP (6.66 gC/m²/year, $p = 0.000$). CO₂ fertilization showed significant positive effects on GPP in Aalmost all the China's subtropical forests showed significant positive effects of CO₂ fertilization on GPP (nearly accounting for 99.48% of the total forest area) (Fig. 4h), suggesting the high sensitivity of forests in this area to elevated CO₂ concentration.

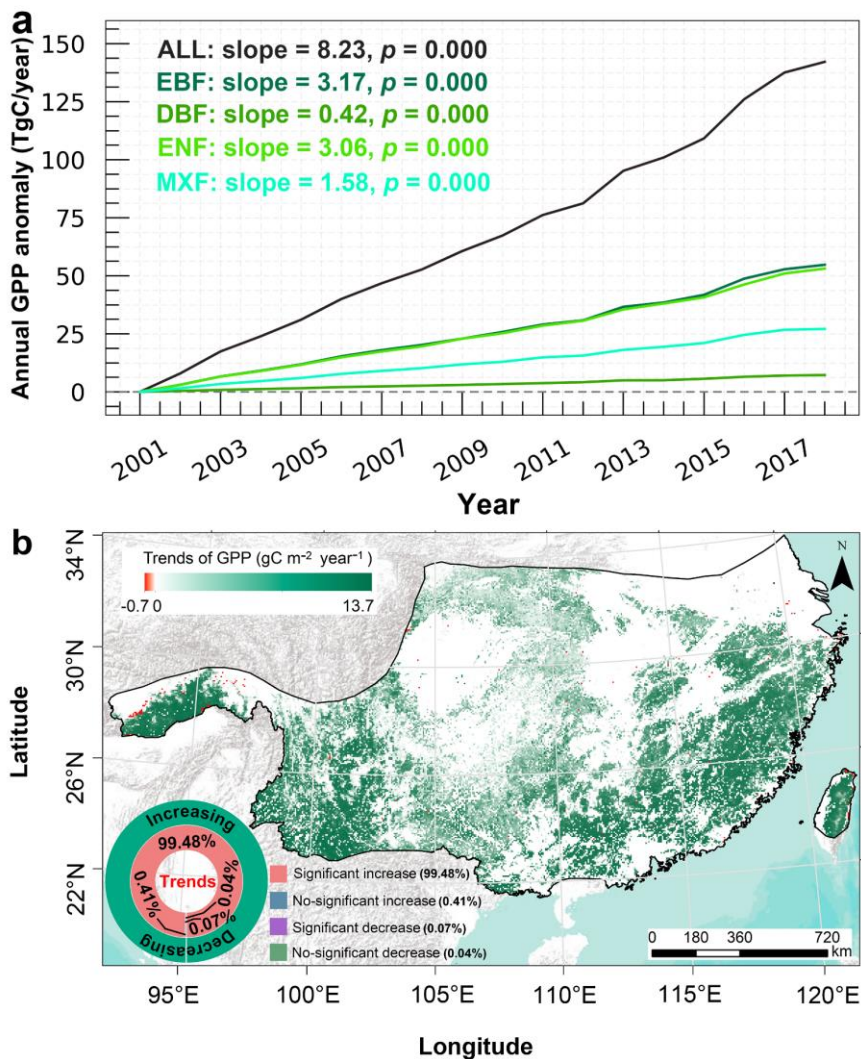
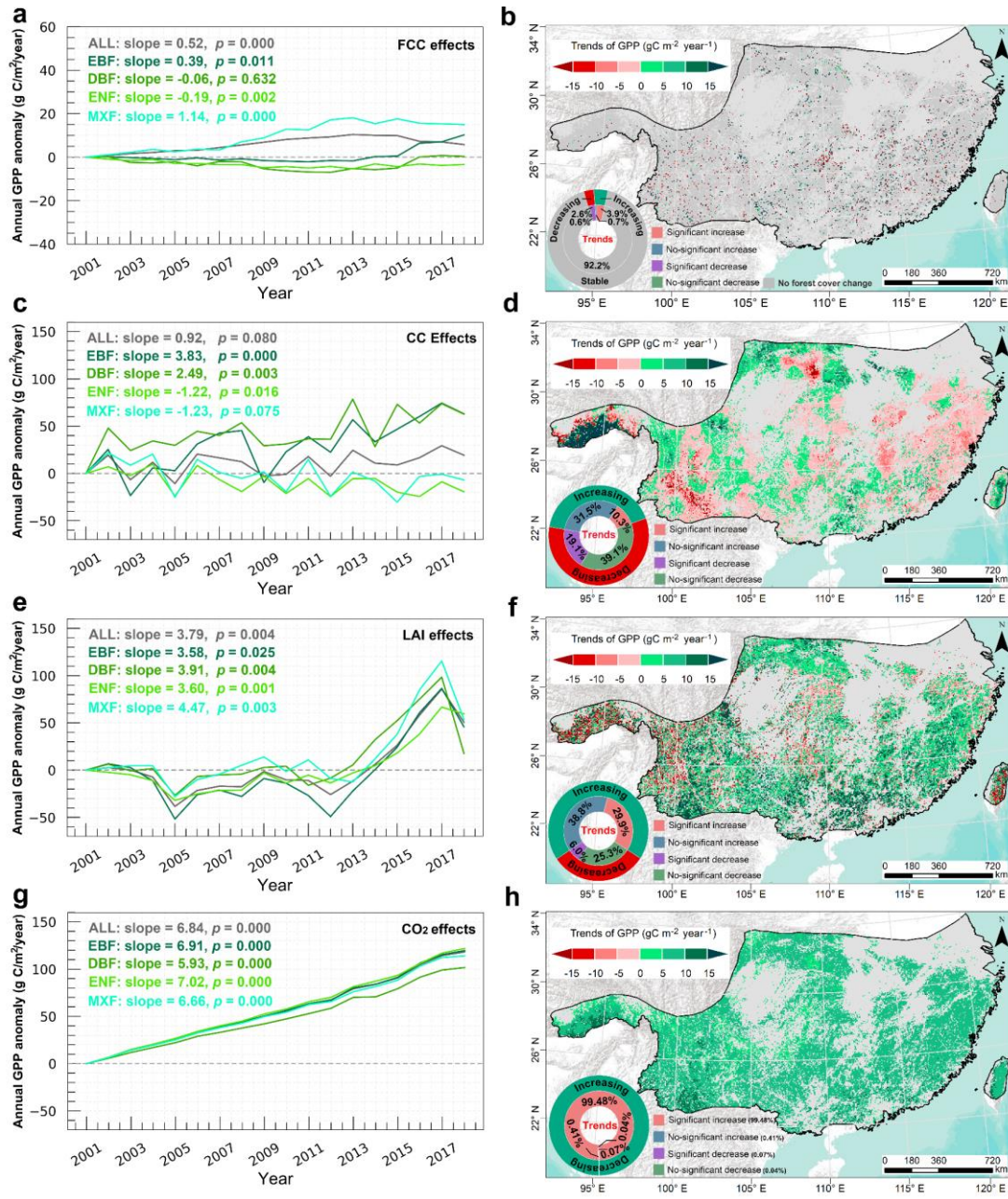


Figure 8 (a) Temporal variation and (b) spatial distribution of the effects of CO₂ fertilization on forest GPP.



495

Figure 4 Temporal variation of the effects of FCC (a), CC (c), LAI (e), and rising CO₂ concentration (g) on annual subtropical forest GPP trends. Spatial distribution of the impacts of FCC (b), CC (d), LAI (f), and rising CO₂ concentration (h) on subtropical forest GPP. Light grey in the study area indicates non-forested areas.

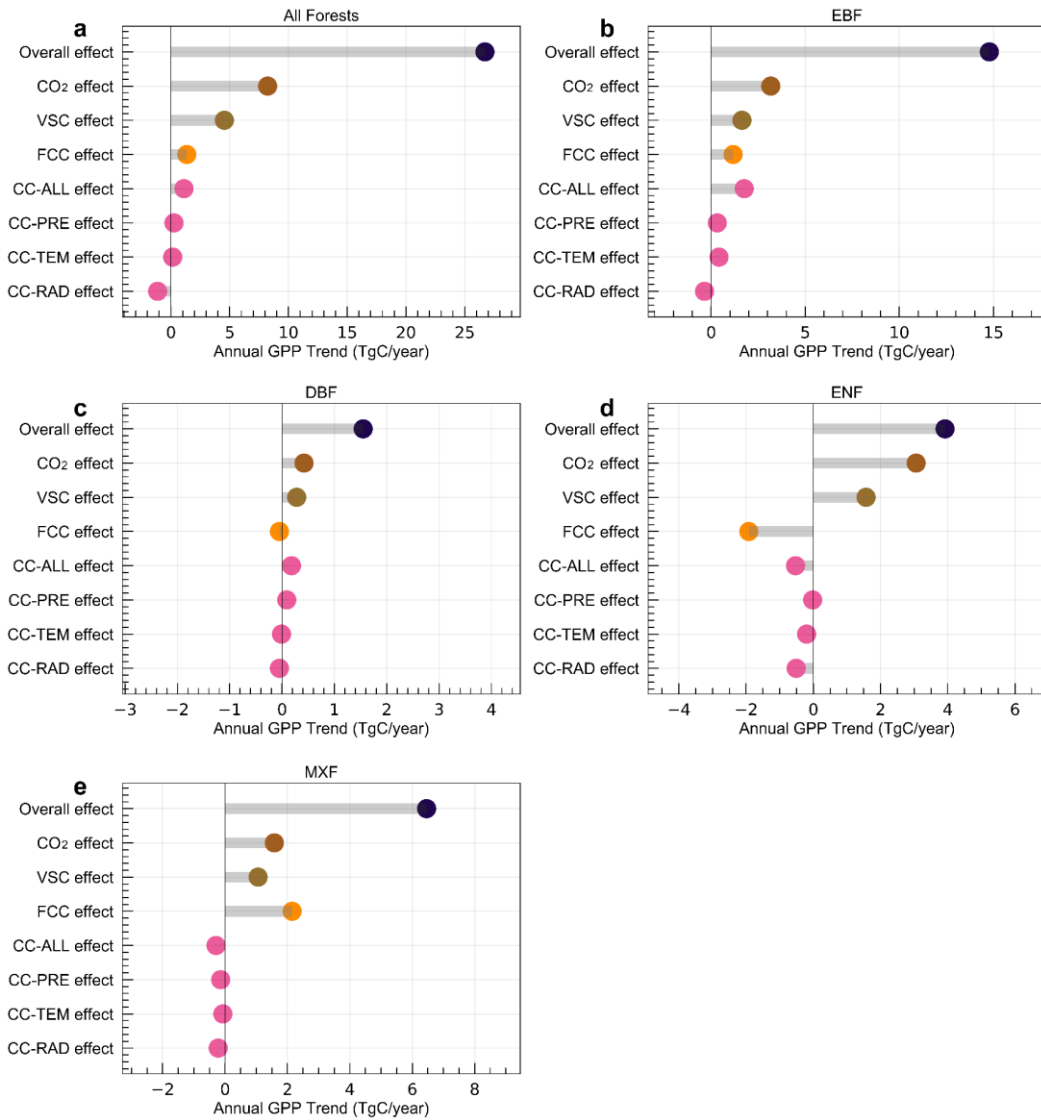
500

3.3.53.3.2 Comparison of the effects among FCC, CC, ~~VSELAI~~, and CO₂ fertilization and the dominant drivers

505

We compared how different drivers contribute to annual trends in different ~~actual~~-subtropical forest GPP (Fig. 95). For all forests together, the enhanced CO₂ concentration made the largest contribution to the overall GPP enhancement, followed by ~~VSELAI~~, CC, and FCC (Fig. 9a5a). In addition to the CO₂ fertilization effect, ~~vegetation-structure-changeLAI~~ was another most dominant contributor to actual subtropical forest GPP increase across the entire and different forest types (Fig. 5Fig-

9b-9e), especially the positive effect of LAI vegetation structure change almost counteracts the negative effect of forest cover change on ENF GPP. The forest cover change, as the dominant factor, mainly contributed to MXF GPP increase (Fig. 9e5e), but resulted in ENF GPP decrease (Fig. 9d5d). Climate change increased the broad-leaved forests (EBF and DBF) GPP (Fig. 9b-5b and 9e5c), but it decreased the ENF GPP and MXF GPP (Fig. 9d-5d and 9e5e). Overall, the EBF in the subtropical region of China has the highest carbon uptake potential in the regulation of the regional carbon cycle (Fig. 9b). Overall, the GPP of EBF in the subtropical region of China experienced the largest growth rate when compared with other forest types (Fig. 5b), and changes in GPP responses to different drivers depending on forest types.



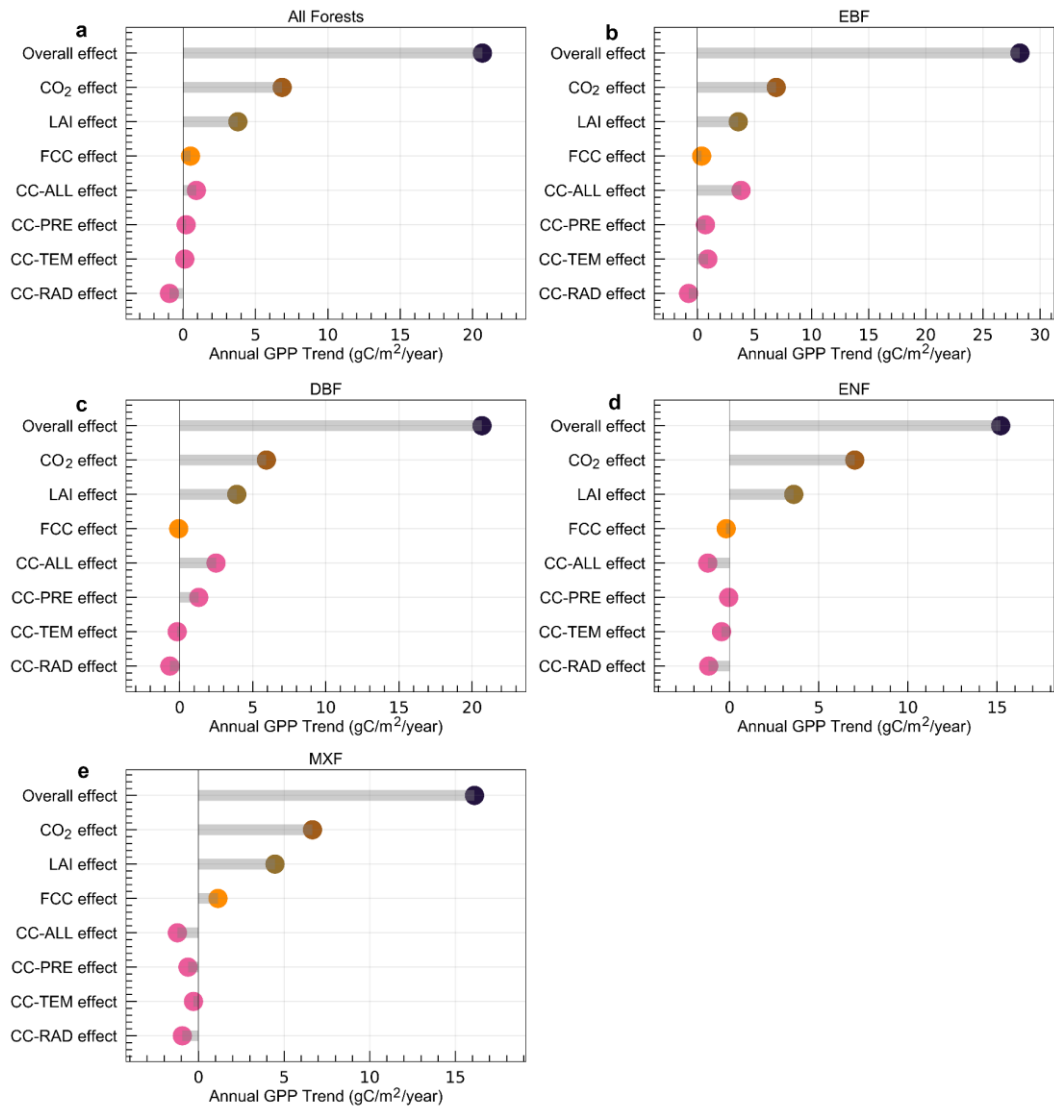
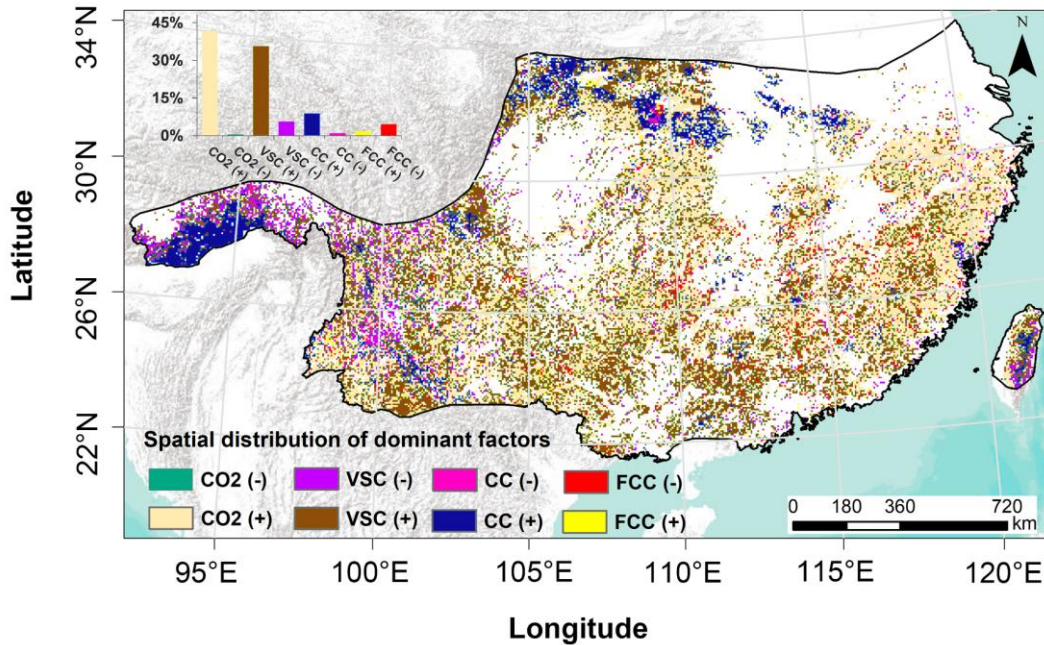


Figure 9-5 Comparison of different drivers to trends in GPP for entire (a) and different forests (b-e). The overall effect denotes the combined effect of all driving factors; the Δ VSC-LAI effect indicates the impact of LAI vegetation structural change on subtropical forest GPP. FCC effect indicates the effect of forest cover change on GPP; CC-ALL, CC-PRE, CC-TEM, and CC-RAD respectively represent the impacts of all climatic factors, precipitation, temperature, and solar radiation on subtropical forest GPP variations.

520

We also investigated the spatial distribution of the effects of dominant factors on subtropical forest GPP trends at every grid cell level as illustrated in Fig. 406. It was observed that a great variation in the spatial distribution of the effects of dominant factors on subtropical forest GPP (Fig. 406). The CO₂ fertilization (41.7%) and Δ VSC-LAI (35.7%) were the two dominant factors of subtropical forest GPP changes in most regions (Fig. 406). However, the CC (8.9%) was the dominant factor driving subtropical forest GPP to increase in the western and northern mountainous areas, and the FCC (4.6%) was the dominant driver of subtropical forest GPP decrease in the east.

525



530

Figure 10.6 Spatial distribution of the effects of dominant factors on subtropical forest GPP changes. (+) and (-) denote the positive and negative effects of these factors on GPP trends, respectively.

4. Discussion

4.1 The effects of the FCC, CC, ~~VSELA~~, and CO₂ fertilization on subtropical forest GPP variation

535

Overall, the actual GPP ~~in both of~~ the entire forest region ~~and, as well as~~ different forest types, displayed an increasing trend over the past two decades (Fig. 43), which is in line with many previous findings (Chen et al., 2021b; He et al., 2019; Li et al., 2022; Tong et al., 2018). The results also confirmed that the subtropical forests in China have a high carbon sequestration potential under the background of global change. However, there were obvious differences ~~among between~~ these factors that contribute to the subtropical forest GPP enhancement.

540

4.1.1 The effect of FCC on subtropical forest GPP

In the past two decades, the Chinese government has made an enormous investment to implement some key ecological restoration programs to improve the forest areas, such as the Grain for Green Program (GGP, initiated in 2000) and the Yangtze and Pearl River Basin Shelterbelt programs (Viña et al., 2016; Zhang et al., 2022). The nationwide field samplings confirmed the increment of vegetation cover and carbon sink via these ecological projects since the end of the 20th century (Lu et al., 2018). Especially, the forest restoration hotspots were observed in the south slope of the Qinling Mountains (Chen et al., 2021b) and the southwest karst region (Tong et al., 2018) of China. In similar regions, we also observed that the positive effect of FCC on GPP ~~increased~~ (Fig. 5e4a-4b). This is due to the increase in the total area of EBF and MXF (Fig. 5a4a), which ~~is are~~ mainly converted from cropland, ~~as shown in the land cover change matrix~~ (Table S6). For example, after the conversion of cropland to MXF in the study area, GPP in the converted area increased by 0.16 Tg C between 2001 and 2018.

550

The previous studies (Chen et al., 2021a; Chen et al., 2021b; Zhang et al., 2022) usually considered different forests in China as a single forest type, ~~which may ignore the negative effect of a specific forest type on forest GPP variations~~ which may ignore the different effects of a specific forest type on forest GPP variations. In this study, we identified the positive effect ($0.52 \text{ gC/m}^2/\text{year}$ ~~$-1.35 \text{ TgC year}^{-1}$~~) of FCC on GPP for all subtropical forest types together. However, disagreements with previous results were also witnessed. The total area of the ENF was ~~reduced~~ lost obviously during the study period in eastern and southern regions, and most of the ENF was converted to MXF (19,040 km²) and cropland (13,100 km²) ~~non-forest lands such as cropland and urban~~ (Table S6), causing large parts of GPP to decrease (Fig. ~~5e4a~~). Therefore, this side effect may ~~be overlooked~~ go unnoticed if different forest types are not considered. For example, the reduction in ENF GPP ($-0.19 \text{ gC/m}^2/\text{year}$) mainly located in the eastern and southern regions was ~~more than~~ offset by the GPP of EBF and MXF (total: $1.53 \text{ gC/m}^2/\text{year}$) in most regions (Fig. 4a-b). Therefore, under the influence of FCC, the entire subtropical forest GPP showed an increasing trend ($0.52 \text{ gC/m}^2/\text{year}$) (Fig. ~~5b4a~~). ~~Additionally, previous studies generally lumped the land cover change and land use change (LUCC) together and concluded that LUCC is a dominant driver for promoting the forest GPP increase in southern China. However, it may largely ignore the huge contribution of land use change (e.g., forest growth and regeneration) to GPP increase, even when forest cover is unchanged, thereby overstating the role of increased forest area in carbon sequestration in China (Chen et al., 2021a). For instance, Zhang et al. (2022) reported that the reduction of forest cover area instead induced GPP to increase during 2001–2010 in a similar study area, which actually benefited from the contribution of the forest growth (i.e., the increase of the LAI) due to reasonable forest management, instead of forest cover change. Therefore, distinguishing the relative contributions of land cover change and land use change to GPP is an essential task.~~

4.1.2 The effect of CC on subtropical forest GPP

Under the combined effect of all climatic factors, an overall increase ($0.92 \text{ gC/m}^2/\text{year}$) in subtropical forest GPP was observed in the study area (Fig. ~~6g4c~~). However, different climatic factors play different roles in regulating the subtropical forest GPP changes (Fig. ~~6a-6FS12~~). The precipitation increased the whole subtropical forest GPP of the entire study area ($0.21 \text{ gC/m}^2/\text{year}$) (Fig. ~~6As12a~~), especially in the northern and western mountains (Fig. S12b). This is because the slight increase in precipitation in these areas, without exceeding a certain threshold, can increase ~~the~~ soil water content and alleviate ~~the impact of~~ drought stress on forest growth, thereby facilitating forest photosynthesis and enhancing the GPP (He et al., 2019; Li et al., 2022). Temperature is another complex driver of forest GPP variation. ~~Many studies suggested that an increment in temperature can benefit the vegetation productivity, or could reduce the vegetation productivity such as the effect of drought. Many studies suggested that an increment in temperature can benefit the vegetation productivity (Myneni, et al., 1997; Nemani, et al., 2003; Song et al., 2022), or could reduce the vegetation productivity due to increased VPD as a result of a high temperature increase (Yuan et al., 2019; Lopez et al., 2021).~~ Our findings also proved that the effect of temperature on subtropical forest GPP varied spatially (Fig. S12d). Most of the region (59.7%) experienced a decline in subtropical forest GPP due to the effects of climate warming, while 40.3% of the subtropical forest GPP located in the western mountains displayed a significant upward trend (Fig. ~~6DS12d~~). This is because the increase in temperature in mountainous areas with high

altitudes can extend the growing season and enhance photosynthesis (Nemani et al., 2003; Piao et al., 2005; Zhang et al., 2014), thereby improving the subtropical forest GPP. The magnitude of GPP increase in the small areas is significantly higher than in other regions because temperature, precipitation and radiation all contribute to GPP increase in these areas (Fig. S12). Although the area of GPP reduction due to climate change is relatively large, the magnitude of its impact is relatively small, resulting in smaller areas with higher magnitude offsetting the larger area of GPP decrease. On the contrary, the solar radiation in this study showed a downward trend (Fig. ~~S9ES11e-f~~). As a direct limiting factor of vegetation growth, the reduction of solar radiation can directly affect forest photosynthesis, thus declining the subtropical forest GPP. As expected, solar radiation in this study declined GPP over 67.2% ~~of GPP~~ of the total area (Fig. ~~6e-6S12f~~), which may be associated with ~~the~~ recent increase in air pollution in China (Chen et al., 2021a; Zhang et al., 2014). The combined effects of these climatic factors caused a positive effect (0.92 gC/m²/year) on the entire subtropical forest GPP, while different forest types showed different responses to climate change (Fig. ~~6g4c~~). For example, ~~climate change has a positive effect on evergreen broadleaved forest GPP, but the negative on evergreen needleleaved forest GPP~~ climate change has a positive effect on the GPP of EBF, but a negative effect on the GPP of ENF. The main reason is that ENF is predominantly located in the eastern and western parts of the subtropics (Fig. 1). In these areas, individual climatic factors (e.g., temperature, precipitation, and solar radiation) or their interactions caused the GPP of ENF to decrease (Fig. 4c-4d), and particularly the solar radiation declined significantly in the eastern region, which led to a decrease in the GPP of ENF in the east. The EBF is mainly distributed in the central and western regions (Fig. 1) where climate change mainly contributes to the increase of EBF GPP (Fig. 4c-4d). Therefore, future measures to combating ~~combate~~ and mitigating ~~mitigate~~ climate change should consider different forest types and their geographical locations.

4.1.3 The effect of VSC-LAI on subtropical forest GPP

As the most important proxy of vegetation ~~structure~~ structural change (VSC) (Chen et al., 2019b; Chen et al., 2021a), LAI can reflect vegetation growth and significantly influence the carbon cycle. Since the 2000s, some key forest protection programs, including the Natural Forest Protection Project (NFPP, initiated in 1998), were carried out in the subtropical region of China (Chen et al., 2020). Due to forest protection and reasonable forest use and management with the support of ecological engineering, forest natural growth has ~~improved~~ increased the LAI (Chen et al., 2020) and further contributed to the GPP increase in China (Tong et al., 2018). A recent study showed that land-use management in China, especially forest management, has contributed significantly to earth greening, accounting for 25% of the increase in global LAI (Chen et al., 2019a). Chen et al. (2019b) estimated the effect of vegetation structural change ~~VSC~~ using the index of LAI on global terrestrial carbon sink since the 1980s, and confirmed that VSC-LAI significantly improved the carbon uptake over the global terrestrial ecosystems, ~~especially~~ Especially, the VSC-LAI also promoted the forest carbon sink in China's subtropical region, but the contribution of different forest VSC-LAI to GPP changes was not revealed. Evidence from our study demonstrated the VSC-LAI as-being the dominant contributor (3.79 gC/m²/year) to the GPP increment of the entire subtropical forests (Fig. ~~74e~~), and also identified the MXF ~~were-as~~ the main contributors to the positive effect of VSC-LAI on GPP changes. Recently, although some studies have ~~also~~ demonstrated the positive effects of VSC-LAI on forest carbon sequestration in China (Chen et al.,

2019b; Chen et al., 2020; Zhang et al., 2022), these studies did not isolate the independent effects of ~~VSC~~
635 LAI on different forest GPP. Currently, some ecological projects in China are aimed at protecting forests,
others are aimed at increasing forest area. Therefore, it has been long debated on how different ecological
projects impact ecosystem services in carbon sequestration (Chen et al., 2020; Yin and Yin, 2010; Yu et
al., 2011). In this study, we designed an experiment to understand the individual impact of ~~VSC~~LAI (i.e.,
only reflecting forest structure change) on subtropical forest GPP changes. The results showed that forest
640 structure change more than forest cover change positively impacted GPP increases in the study area (Fig.
4, Fig. 5Fig-9a), implying that forest protection projects in the subtropical region of China may have
greater carbon uptake potential. Consistent with our study period (2001–2018), Chen et al. (2021b) also
reported an increase in vegetation carbon sequestration in China based on the two indicators of GPP and
NPP, especially with an accelerated increase in carbon sequestration potential after 2010. They showed
645 that GPP and NPP in China increased obviously at the rate of 49.1–53.1 TgC/yr² and 22.4–24.9 TgC/yr²,
respectively. The significant increase of subtropical forest GPP and NPP was highly attributed to human
activities (e.g., ecological restoration projects) in southern and eastern China, especially the human-
induced NPP gains can offset the climate-induced NPP losses in southern China.

4.1.4 The effect of CO₂ fertilization on subtropical forest GPP

650 The carbon sequestered by vegetation through photosynthesis in a given unit of space and time,
i.e., GPP, forms the fundamental part of the carbon cycle (Monteith 1972). GPP is a crucial indicator for
estimating the carbon sequestration capacity of ecosystems (Chen et al., 2021b; Ma et al., 2019), which
reflects the largest carbon sequestered by plant photosynthesis (Christian et al., 2010; Xu et al., 2019).
Moreover, GPP drives land carbon sequestration and partly offsets anthropogenic CO₂ emission, which
655 significantly affects global carbon balance and climate change (Running et al., 2008). In this study, we
investigated the the impact of rising CO₂ concentration on GPP in subtropical forests in China. Our
results also suggested that CO₂ fertilization was the major contributor to the overall forest GPP increase
in China's subtropical region (6.84 gC/m²/year8.23 TgC year⁻¹) (Fig. 84g and Fig. 5). Elevated CO₂
concentration can enrich the intercellular CO₂ and stimulate vegetation photosynthetic rates, thereby
660 enhancing vegetation productivity. Recent studies suggested that the CO₂ fertilization effect was the main
driver in promoting global or regional vegetation productivity (Chen et al., 2022a; Chen et al., 2019b;
Schimel et al., 2015; Xie et al., 2020). This was also confirmed by the results of free-air CO₂ enrichment
(FACE) experiments (Norby et al., 2010) and a previous study using terrestrial biosphere models, remote
sensing-based methods, ecological optimality theory and an emergent constraint based on global carbon
665 budget estimates (Keenan et al., 2023) This was also confirmed by observations of the globally
distributed eddy covariance networks (Chen et al., 2022a; Zhan et al., 2022). The forests in China are
characterized by relatively young stand age (< 40 years old) due to a large number of new plantations,
and thus China's forest carbon sequestration potential may continue to increase in the near future due to
the rising CO₂ concentration (Yao et al., 2018a). ~~However, there is a lack of dependable and spatially~~
670 ~~explicit CO₂ concentration data, especially in China, we only used the annual mean CO₂ concentrations~~
~~from the Mauna Loa Observatory to represent the spatially homogeneous CO₂ concentrations in the study~~
~~area and to drive the model, which may spatially overestimate or underestimate the effect of CO₂~~
~~fertilization on forest GPP (Peng et al., 2022), although it may reasonable to use spatially uniform and~~

675 annual average CO₂ concentration to the estimation of large-scale GPP (Chen et al., 2022a; Chen et al., 2021a).

4.2 Model and Uncertainties

680 In the BEPS model, the LAI is separated into two parts including the LAI of sunlit and shaded leaves, which are adopted to calculate the photosynthesis at leaf level (sunlit and shaded leaves) based on the FvCB photosynthesis model (Farquhar et al., 1980), and further compute the GPP at canopy level by adding the photosynthesis rates of sunlit and shaded leaves. Moreover, the Ball-Berry equation (Ball et al., 1987) was used in the model to calculate the stomatal conductance of sunlit and shaded leaves, which influenced the intercellular CO₂, the photosynthesis rate, and evapotranspiration (ET). Therefore, the LAI directly determined the allocation of light and water availability and influenced the gross photosynthesis rate of the sunlit and shaded leaves. The LAI may impact its contribution to GPP variations through these processes. The atmospheric CO₂ concentration affects the intercellular CO₂ through the stomatal conductance, which, together with temperature and maximum carboxylation rate (V_{cmax}), determines the Rubisco-limited (A_c) and RuBP-limited (A_j) gross photosynthesis rate in the model. Over the past few decades, the CO₂ concentrations continuously increased and reached the current level of over 400 ppm. Elevated atmospheric CO₂ concentration can increase photosynthesis by accelerating the rate of carboxylation, thereby influencing the GPP changes. Additionally, solar radiation variability would directly influence the potential electron transport rate and thus regulate the RuBP-limited (A_j) gross photosynthetic rate. The temperature in the model directly impacts the V_{cmax} and the CO₂ compensation point without dark respiration (Γ), thereby determining the gross photosynthesis rate. The temperature positively affects the V_{cmax} when it is below the optimal temperature. However, when the temperature exceeds the optimal temperature, V_{cmax} will not continue to increase with the temperature. Therefore, changes in temperature in the model may have a positive or negative impact on GPP.

700 It should be noted that changes in LAI could be influenced by both climatic factors and elevated atmospheric CO₂ concentration (Chen et al., 2019; Chen et al., 2021a; Sun et al., 2022). Previous studies reported that the elevated atmospheric CO₂ concentration was the dominant driver of global LAI increase, and there are also regional differences in the impact mechanism of climate factors on LAI changes (Zhu et al., 2016; Zhu et al., 2017), thereby influencing the GPP dynamics. Moreover, the interactions between these driving factors can also influence the LAI, and even the interactive impacts of these factors on LAI may offset each other. For instance, rising CO₂ concentration and solar radiation can affect temperature and VPD (Chen et al., 2021a). High VPD leads to plants to close their stomata, resulting in lower intercellular CO₂ concentrations in the leaves, which reduces the rate of photosynthesis (Yuan et al., 2019). Additionally, changes in LAI can feed back to the climate through biogeochemical and biogeophysical processes (Li et al., 2023). There is a bidirectional interaction between vegetation and the atmosphere, and the relationship between vegetation dynamics and driving factors is complicated. The current methods used in this study cannot elucidate the complex interactions of the climate factors and elevated CO₂ concentration on LAI changes, which may bring some uncertainties to our results.

710 In this study, we used the process-based BEPS model to simulate subtropical forest GPP of the subtropical region China. We first used the V_{cmax25} product retrieved from remote sensing data (i.e., leaf

chlorophyll content) to replace the constant value of the $V_{\text{cmax}25}$ in the model. Wang et al. (2019), Luo et al. (2018), and Croft et al. (2017) indicated that the use of the remotely sensed leaf chlorophyll content to invert $V_{\text{cmax}25}$ can improve the accuracy of GPP simulation in evergreen conifer forests and a temperate deciduous forest. Our results suggested that the BEPS model with spatial varying $V_{\text{cmax}25}$ values can also reach reasonable simulation of subtropical forest GPP over spatiotemporal scales (Fig. 2, Fig. S1-S6). Incorporating the spatial variation of the $V_{\text{cmax}25}$ inverted by remotely sensed data into the process-based model does not require its pre-calibration (Chen et al., 2022b), thus it has great potential to be applied to areas with few flux sites, such as China's subtropical forest area. However, the $V_{\text{cmax}25}$ retrieved from remote sensing data is still in the early developing stage (Chen et al., 2022b; Luo et al., 2019). For example, the $V_{\text{cmax}25}$ product used in this study was mainly generated by the MODIS surface reflectance, thus the data quality of the surface reflectance may cause the uncertainty in $V_{\text{cmax}25}$ product. The uncertainties in MODIS reflectance datasets can arise from sensor calibration issues, cloud contamination, atmospheric correction errors, etc. Changes in the reflectance could result in large changes in the modelled chlorophyll values, thereby affecting the $V_{\text{cmax}25}$ product. Additionally, the $V_{\text{cmax}25}$ was produced by a semi-mechanistic model (Friend., 1995), and the key parameter K_{cat}^{25} (the Rubisco turnover rate at 25 °C) in the model would bring uncertainties in modeling $V_{\text{cmax}25}$, because current ground-based data are still rarely used for calibration of this parameter and validation of the $V_{\text{cmax}25}$ products (Lu et al., 2022; Chen et al., 2022b), and the high-accuracy of spatiotemporal variability of $V_{\text{cmax}25}$ products at global and regional scales should be further explored.

~~In the BEPS model, the LAI is the most important input for carbon fluxes simulation. Previous studies reported large differences in trend and magnitude between existing LAI products over the globe (Fang et al., 2019; Jiang et al., 2017; Liu et al., 2018). Therefore, only the GLASS LAI was used in this study to simulate GPP, which may cause some uncertainty. However, Liu et al. (2018) estimated the accuracy of different satellite derived LAI products for the simulation of carbon and water fluxes in China's forests based on the BEPS model, and proved that GLASS LAI showed higher accuracy in simulating forest GPP than other LAI products (e.g., FSGOM LAI and MODIS LAI). The consistent conclusions also have been reported in other studies (Chen et al., 2021a; Jiang et al., 2017; Xie et al., 2019). Therefore, it was reasonable to use GLASS LAI as input to model forest GPP in this study.~~

~~There are large differences between the available land cover data, such as ESA CCI land cover data (ESA, 2017) and MODIS land cover data (Sulla-Menashe et al., 2019), which were mainly caused by the discrepancies in the definition of forest and divergent data sources (Li et al., 2016; Magdon et al., 2014). Eventually, the use of different land cover data may also lead to uncertainty in the estimate of the regional total GPP. The satellite-derived ESA CCI land cover used in this study may suffer from cloud contamination, satellite signal aliasing, and uncertainty from algorithmic flaws that affect the accuracy of forest cover mapping (Dong et al., 2012). Yang et al. (2017b) systematically evaluated the accuracy of different land cover data in China, showing that ESA CCI data has higher accuracy, especially compared to the commonly used MODIS land cover data. Currently, remote sensing is still considered to be the only effective tool for land cover mapping at large scales, and more precise remote sensing is still needed in the future. Besides, assessing the uncertainties and discrepancies in carbon flux simulations~~

~~from different land cover data will be the next research work~~

5. Conclusions

In this study, the BEPS model was used to simulate the subtropical forest GPP. We examined the performance of the BEPS model in simulating subtropical forest GPP, which can reach a high accuracy of GPP simulation in the subtropical forest region of China. A significant increasing trend ($20.67 \text{ gC/m}^2/\text{year}$, $p < 0.001$) was detected in the subtropical forest GPP over the past two decades, indicating that sustained increase in the carbon sink potential of the subtropical forests under the background of global change, especially the evergreen broadleaved forest (EBF) ~~EBF is being~~ the biggest contributor ($28.24 \text{ gC/m}^2/\text{year}$ ~~14.78 TgC year⁻¹~~, $p < 0.001$) to total GPP enhancement of the entire subtropical forests. We designed different groups of simulations to examine the individual and combined impacts of ~~FCC~~ forest cover change (FCC), ~~CC~~ climate change (CC), ~~VSC~~ leaf area index (LAI), and CO₂ fertilization on inter-annual trends in subtropical forest GPP. There are obvious differences in drivers of different subtropical forest GPP variations.

Although the CO₂ fertilization effect is the largest contributor to the overall subtropical forest GPP increase, the VSC-LAI was another most important and not negligible contributor to subtropical forest GPP growth in China. The FCC mainly contributed to the mixed forest (MXF) ~~MXF GPP increase~~ ($1.14 \text{ gC/m}^2/\text{year}$ ~~2.15 TgC year⁻¹~~, $p < 0.001$) and EBF GPP ($0.39 \text{ gC/m}^2/\text{year}$, $p < 0.001$) increase, but induced the evergreen needle-leaved forest (ENF) ~~ENF GPP~~ to decrease ($-0.19 \text{ gC/m}^2/\text{year}$ ~~1.92 TgC year⁻¹~~, $p < 0.001$). The CC also increased the EBF and deciduous broadleaved forest (DBF) ~~DBF GPP~~, but it decreased the ENF and MXF GPP. Especially, the ~~forest~~-EBF and DBF GPP in this region are very sensitive ($p < 0.05$) to CC. Therefore, we emphasized that the mitigation of climate change and carbon emissions through forests should consider their different types. Furthermore, our results highlighted the VSC-LAI effect, which was greater than ~~the effects that~~ of FCC, was the important driver of the subtropical forest GPP enhancement, suggesting that forest use and management have a more significant positive impact on GPP increase than forest cover change in the study area. It may attribute to the implementation of China's forest protection and restoration programs. ~~Overall, with the support of the government's ecological programs, rational solutions for managing and improving forest structure and function, rather than continuously increasing forest area, may facilitate and maintain the sustainability of the carbon sequestration potential in the study area.~~

Acknowledgments

This work is jointly supported by the National Natural Science Foundation of China (Grant No. 42171025), the Fonds Wetenschappelijk Onderzoek (FWO Grant n° G018319N), and the program of the China Scholarships Council (Grant No. 202106380124).

Data Availability statement

We obtained the flux tower data from the ChinaFLUX network (<http://www.chinaflux.org/>), the GLASS LAI from the University of Maryland (<http://www.glass.umd.edu/Contact.html>), the $V_{\text{cmax}25}$ products from the National Ecosystem Science Data Center, National Science & Technology Infrastructure of

China (<http://www.nesdc.org.cn>), the meteorological datasets from the National Tibetan Plateau Third Pole Environment Data Center (<https://data.tpdc.ac.cn/en/>), the annual land use/cover datasets and the CCI LC user tool from the European Space Agency (ESA) (<http://maps.elie.ucl.ac.be/CCI/viewer/>), the soil data from the FAO (<https://doi.org/10.3334/ORNLDAAAC/1247>), and the atmospheric CO₂ data from the National Oceanic and Atmospheric Administration's Earth System Research Laboratories (<https://gml.noaa.gov/obop/mlo/>).

795 **Author contributions**

Conceptualization, methodology, data analysis, writing— original draft, writing—review and editing: TC; conceptualization, methodology, writing— original draft, writing—review and editing: FM. Model, writing— original draft, writing—review and editing: MP. Conceptualization, funding acquisition, project administration, writing—review and editing: GT. Visualization, writing—review and editing: YY.
800 Conceptualization, data analysis, funding acquisition, project administration, writing— original draft, writing—review and editing: HV. All authors have read and agreed to the published version of the manuscript.

Supplement

The supplement related to this article is available online.

805 **Competing interests**

The authors declare that they have no known competing financial interests or personal relationships that could have appeared to influence the work reported in this paper.

Disclaimer

Publisher's note: Copernicus Publications remains neutral with regard to jurisdictional claims in
810 published maps and institutional affiliations

References

- Barman, R., Jain, A.K. and Liang, M., 2014. Climate-driven uncertainties in modeling terrestrial gross primary production: a site level to global-scale analysis. *Global Change Biology*, 20(5): 1394-1411.
- 815 [Ball, J.T., et., 1987. A model predicting stomatal conductance and its contribution to the control of photosynthesis under different environmental conditions. J. Biggins \(Ed.\). Progress in Photosynthesis Research: Volume 4 Proceedings of the VIIth International Congress On Photosynthesis Providence, Rhode Island, USA, August 10–15, 1986. Springer Netherlands, Dordrecht, pp. 221–224.](#)
- 820 Beer, C. et al., 2010. Terrestrial Gross Carbon Dioxide Uptake: Global Distribution and Covariation with Climate. *Science*, 329(5993): 834-838.
- [Camberlin, P., et al., 20007. Determinants of the interannual relationships between remote sensed photosynthetic activity and rainfall in tropical Africa. Remote sensing of environment, 106, 199–216.](#)
- 825 Chen, C. et al., 2019a. China and India lead in greening of the world through land-use management. *Nature Sustainability*, 2: 122-129.

- ~~Chen, C., Riley, W.J., Prentice, I.C. and Keenan, T.F., 2022a. CO₂ fertilization of terrestrial photosynthesis inferred from site to global scales. *Proceedings of the National Academy of Sciences*, 119(10): e2115627119.~~
- 830 Chen, J.M., Ju, W., Ciais, P., Viovy, N. and Lu, X., 2019b. Vegetation structural change since 1981 significantly enhanced the terrestrial carbon sink. *Nature Communications*, 10(1): 4259.
- Chen, J.M., Liu, J., Cihlar, J. and Goulden, M.L., 1999. Daily canopy photosynthesis model through temporal and spatial scaling for remote sensing applications. *Ecological Modelling* 124(2-3): 99–119.
- 835 Chen, J.M. et al., 2012. Effects of foliage clumping on the estimation of global terrestrial gross primary productivity. *Global Biogeochemical Cycles*, 26(1): GB1019.
- Chen, J.M. et al., 2022b. Global datasets of leaf photosynthetic capacity for ecological and earth system research. *Earth System Science Data*, 14(9): 4077-4093.
- 840 Chen, S. et al., 2021a. Vegetation structural change and CO₂ fertilization more than offset gross primary production decline caused by reduced solar radiation in China. *Agricultural and Forest Meteorology*, 296: 108207.
- Chen, Y. et al., 2020. Afforestation promotes the enhancement of forest LAI and NPP in China. *Forest Ecology and Management*, 462: 117990.
- 845 Chen, Y. et al., 2021b. Accelerated increase in vegetation carbon sequestration in China after 2010: A turning point resulting from climate and human interaction. *Global Change Biology*, 27(22): 5848-5864.
- ~~Christian, B., et al., 2010. Terrestrial gross carbon dioxide uptake: Global distribution and covariation with climate. *Science*, 329 (5993), 834–838.~~
- 850 CMA, 2018. China Greenhouse Gas Bulletin: The State of Greenhouse Gases in the Atmosphere Based on Chinese and Global Observations before 2017. <http://www.cma.gov.cn/en2014/news/News/201901/P020190122575481732415.pdf>.
- Croft, H. et al., 2017. Leaf chlorophyll content as a proxy for leaf photosynthetic capacity. *Global Change Biology*, 23: 3513–3524.
- 855 Dong, J. et al., 2012. A comparison of forest cover maps in Mainland Southeast Asia from multiple sources: PALSAR, MERIS, MODIS and FRA. *Remote Sensing of Environment*, 127: 60-73.
- ESA, 2017. Land Cover CCI: Product User Guide Version 2.0. [Online]. Available: https://maps.elie.ucl.ac.be/CCI/viewer/download/ESACCI-LC-Ph2-PUGv2_2.0.pdf [Accessed January 15th 2022].
- 860 ~~Farquhar, et al., 1980. A biochemical model of photosynthetic CO₂ assimilation in leaves of C₃ species. *Planta* 149, 78–90.~~
- Fang, H., Baret, F., Plummer, S. and Schaepman-Strub, G., 2019. An Overview of Global Leaf Area Index (LAI): Methods, Products, Validation, and Applications. *Reviews of Geophysics*, 57(3): 739-799.
- 865 Fang, J. et al., 2014. Forest biomass carbon sinks in East Asia, with special reference to the relative contributions of forest expansion and forest growth. *Global Change Biology*, 20(6): 2019–2030.
- Fang, J., Tang, Y. and Son, Y., 2010. Why are East Asian ecosystems important for carbon cycle research? *Sci China Life Sci*, 53(7): 753–756.
- Fang, J., Yu, G., Liu, L., Hu, S. and Chapin, F.S., 2018. Climate change, human impacts, and carbon

- sequestration in China. *Proceedings of the National Academy of Sciences*, 115(16): 4015-4020.
- 870 FAO, 2012. Harmonized World Soil Database (version 1.2). Food Agriculture Organization, Rome, Italy and IIASA, Laxenburg, Austria (<http://webarchive.iiasa.ac.at/Research/LUC/External-World-soil-database/HTML/>).
- Feng, X. et al., 2007. Net primary productivity of China's terrestrial ecosystems from a process model driven by remote sensing. *Journal of Environmental Management*, 85(3): 563-573.
- 875 [Forzieri, G., Dakos, V., McDowell, N.G., Ramdane, A. and Cescatti, A., 2022. Emerging signals of declining forest resilience under climate change. *Nature*, 608\(7923\): 534-539.](#)
- [Friend, A., 1995. PGEN: an integrated model of leaf photosynthesis, transpiration, and conductance *Ecological Modelling*, 77: 233-55.](#)
- 880 Friedlingstein, P. et al., 2022. Global Carbon Budget 2021. *Earth System Science Data*, 14(4): 1917-2005.
- Fyllas, N.M. et al., 2017. Solar radiation and functional traits explain the decline of forest primary productivity along a tropical elevation gradient. *Ecology Letters*, 20(6): 730-740.
- Gao, T., Wang, H.J. and Zhou, T., 2017. Changes of extreme precipitation and nonlinear influence of climate variables over monsoon region in China. *Atmospheric Research*, 197: 379-389.
- 885 [Grossiord, C., et al., 2020. Plant responses to rising vapor pressure deficit. *New Phytologist*, 226\(6\), 1550-1566.](#)
- He, H. et al., 2021a. Reference carbon cycle dataset for typical Chinese forests via colocated observations and data assimilation. *Scientific Data*, 8(1): 42.
- 890 He, H. et al., 2019. Altered trends in carbon uptake in China's terrestrial ecosystems under the enhanced summer monsoon and warming hiatus. *National Science Review*, 6(3): 505-514.
- He, J. et al., 2020. The first high-resolution meteorological forcing dataset for land process studies over China. *Scientific Data*, 7(1): 25.
- 895 He, Q. et al., 2021b. Drought Risk of Global Terrestrial Gross Primary Productivity Over the Last 40 Years Detected by a Remote Sensing-Driven Process Model. *Journal of Geophysical Research: Biogeosciences*, 126(6): e2020JG005944.
- Huang, J. et al., 2021. Characterizing the river water quality in China: Recent progress and on-going challenges. *Water Research*, 201: 117309.
- Jiang, C. et al., 2017. Inconsistencies of interannual variability and trends in long-term satellite leaf area index products. *Global Change Biology*, 23(10): 4133-4146.
- 900 Ju, W. et al., 2006. Modelling multi-year coupled carbon and water fluxes in a boreal aspen forest. *Agricultural and Forest Meteorology*, 140(1-4): 136-151.
- [Keenan, T.F., et al., 2016. Recent pause in the growth rate of atmospheric CO₂ due to enhanced terrestrial carbon uptake. *Nature Communications*, 7, 13428.](#)
- 905 [Keenan, T. F., et al., 2023. A constraint on historic growth in global photosynthesis due to rising CO₂. *Nature Climate Change*, 13: 1376-1381.](#)
- Li, C. et al., 2014. A Circa 2010 Thirty Meter Resolution Forest Map for China. *Remote Sensing*, 6(6): 5325-5343.
- [Li, H et al., 2021. Regional contributions to interannual variability of net primary production and climatic](#)

[attributions. Agricultural and Forest Meteorology, 303, 108384.](#)

910 Li, W. et al., 2016. Major forest changes and land cover transitions based on plant functional types derived from the ESA CCI Land Cover product. *International Journal of Applied Earth Observation and Geoinformation*, 47: 30-39.

Li, Y., Zhang, Y. and Lv, J., 2022. Interannual variations in GPP in forest ecosystems in Southwest China and regional differences in the climatic contributions. *Ecological Informatics*, 69: 101591.

915 [Li, Y., et al., 2023. Biophysical impacts of earth greening can substantially mitigate regional land surface temperature warming. Nature Communications,14, 121.](#)

Liu, J., Chen, J.M., Cihlar, J. and Chen, W., 1999. Net primary productivity distribution in the BOREAS region from a process model using satellite and surface data. *Journal of Geophysical Research: Atmospheres*, 104(D22): 27735-27754.

920 Liu, J., Chen, J.M., Cihlar, J. and PARK, W.M., 1997. A process-based boreal ecosystem productivity simulator using remote sensing inputs. *Remote Sensing of Environment*, 62(2): 158-175.

Liu, Y. et al., 2013a. Changes of net primary productivity in China during recent 11 years detected using an ecological model driven by MODIS data. *Frontiers of Earth Science*, 7(1): 112-127.

925 Liu, Y. et al., 2016. Recent trends in vegetation greenness in China significantly altered annual evapotranspiration and water yield. *Environmental Research Letters*, 11(9): 094010.

Liu, Y. et al., 2015. Water use efficiency of China's terrestrial ecosystems and responses to drought. *Sci Rep*, 5: 13799.

Liu, Y. et al., 2018. Satellite-derived LAI products exhibit large discrepancies and can lead to substantial uncertainty in simulated carbon and water fluxes. *Remote Sensing of Environment*, 206: 174-188.

930 Liu, Y. et al., 2013b. Evapotranspiration and water yield over China's landmass from 2000 to 2010. *Hydrology and Earth System Sciences*, 17(12): 4957-4980.

Liu, Y. et al., 2014. Impacts of droughts on carbon sequestration by China's terrestrial ecosystems from 2000 to 2011. *Biogeosciences*, 11(10): 2583-2599.

935 Lu, F. et al., 2018. Effects of national ecological restoration projects on carbon sequestration in China from 2001 to 2010. *Proceedings of the National Academy of Sciences*, 115(16): 4039-4044.

Lu, X., Croft, H., Chen, J.M., Luo, Y. and Ju, W., 2022. Estimating photosynthetic capacity from optimized Rubisco–chlorophyll relationships among vegetation types and under global change. *Environmental Research Letters*, 17(1): 014028.

940 Lu, X. et al., 2020. Maximum Carboxylation Rate Estimation With Chlorophyll Content as a Proxy of Rubisco Content. *Journal of Geophysical Research: Biogeosciences*, 125(8): e2020JG005748.

[Lopez, J., et al., 2021. Systemic effects of rising atmospheric vapor pressure deficit on plant physiology and productivity. Global Change Biology, 27, 1704–1720.](#)

945 Luo, X. et al., 2018. Incorporating leaf chlorophyll content into a two-leaf terrestrial biosphere model for estimating carbon and water fluxes at a forest site. *Agricultural Forest Meteorology*, 248: 156-168.

Luo, X., Croft, H., Chen, J.M., He, L. and Keenan, T.F., 2019. Improved estimates of global terrestrial photosynthesis using information on leaf chlorophyll content. *Global Change Biology*, 25(7): 2499-2514.

Ma, J. et al., 2019. Trends and controls of terrestrial gross primary productivity of China during 2000–

- 950 2016. *Environmental Research Letters*, 14(8): 084032.
- Ma, J., Yan, X., Dong, W. and Chou, J., 2015. Gross primary production of global forest ecosystems has been overestimated. *Scientific Reports*, 5(1): 10820.
- Magdon, P., Fischer, C., Fuchs, H. and Kleinn, C., 2014. Translating criteria of international forest definitions into remote sensing image analysis. *Remote Sensing of Environment*, 149: 252-262.
- 955 Mathias, J.M. and Trugman, A.T., 2022. Climate change impacts plant carbon balance, increasing mean future carbon use efficiency but decreasing total forest extent at dry range edges. *Ecology Letters*, 25(2): 498-508.
- Matsushita, B. and Tamura, M., 2002. Integrating remotely sensed data with an ecosystem model to estimate net primary productivity in East Asia. *Remote Sensing of Environment*, 81(1): 58-66.
- 960 Mo, X., Liu, S., Chen, X. and Hu, S., 2018. Variability, tendencies, and climate controls of terrestrial evapotranspiration and gross primary productivity in the recent decade over China. *Ecohydrology*, 11(4): e1951.
- [Monteith, J. L., 1972. Solar-radiation and productivity in tropical ecosystems. *Journal of Applied Ecology*, 9\(3\), 747-766.](#)
- 965 [Moore, C.E., et al., 2021. The effect of increasing temperature on crop photosynthesis: from enzymes to ecosystems. *Journal of Experimental Botany*, 72 \(8\), 2822-2844.](#)
- [Myneni, R. B., et al., 1997. Increased plant growth in the northern high latitudes from 1981 to 1991. *Nature*, 386, 698–702.](#)
- Nemani, R.R. et al., 2003. Climate-Driven Increases in Global Terrestrial Net Primary Production from 1982 to 1999. *Science*, 300: 1560-1563.
- 970 [Nie, C., et al., 2023. The Spatio-Temporal Variations of GPP and Its Climatic Driving Factors in the Yangtze River Basin during 2000–2018. *Forests*, 14\(9\):1898.](#)
- [Norby, R. J., et al., 2010. CO₂ enhancement of forest productivity constrained by limited nitrogen availability. *Proceedings of the National Academy of Sciences*, 107, 19368–19373.](#)
- 975 Pan, Y. et al., 2011. A large and persistent carbon sink in the world's forests. *Science*, 333(6045): 988-993.
- Peng, J. et al., 2022. Overestimated Terrestrial Carbon Uptake in the Future Owing to the Lack of Spatial Variations CO₂ in an Earth System Model. *Earth's Future*, 10: e2021EF002440.
- Peng, J. et al., 2021. Incorporating water availability into autumn phenological model improved China's terrestrial gross primary productivity (GPP) simulation. *Environmental Research Letters*, 16(9): 094012.
- 980 [Piao, S. et al., 2020. Characteristics, drivers and feedbacks of global greening. *Nature Reviews Earth & Environment*, 1: 14-27.](#)
- Piao, S. et al., 2005. Changes in vegetation net primary productivity from 1982 to 1999 in China. *Global Biogeochemical Cycles*, 19(2): GB2027.
- 985 Reichstein, M. et al., 2005. On the separation of net ecosystem exchange into assimilation and ecosystem respiration: review and improved algorithm. *Global Change Biology*, 11(9): 1424-1439.
- Running, S.W. and Coughlan, J.C., 1988. A general model of forest ecosystem processes for regional applications I. Hydrologic balance, canopy gas exchange and primary production processes. *Ecological Modelling*, 42(2): 125-154.
- 990

- Running, S.W., Mu, Q. and Zhao, M., 2015. MOD17A2H MODIS/Terra Gross Primary Productivity 8-Day L4 Global 500m SIN Grid. NASA LP DAAC. <http://doi.org/10.5067/MODIS/MOD17A2H.006>.
- [Running, S.T., 2008. Ecosystem Disturbance, Carbon, and Climate. Science, 321 \(5889\), 652-653.](#)
- 995 Schimel, D., Stephens, B.B. and Fisher, J.B., 2015. Effect of increasing CO₂ on the terrestrial carbon cycle. Proceedings of the National Academy of Sciences, 112(2): 436-41.
- [Shang et al., 2023. China's current forest age structure will lead to weakened carbon sinks in the near future. The Innovation, 4 \(6\), 100515.](#)
- 1000 [Shevliakova E., et al., 2013. Historical warming reduced due to enhanced land carbon uptake. Proceedings of the National Academy of Sciences, 110,16730–16735.](#)
- [Siddik, M.A., et al., 2019. Responses of indica rice yield and quality to extreme high and low temperatures during the reproductive period. European Journal of Agronomy, 106, 30-38.](#)
- 1005 Sprintsin, M., Chen, J.M., Desai, A. and Gough, C.M., 2012. Evaluation of leaf-to-canopy upscaling methodologies against carbon flux data in North America. Journal of Geophysical Research: Biogeosciences, 117: G01023.
- Sulla-Menashe, D., Gray, J.M., Abercrombie, S.P. and Friedl, M.A., 2019. Hierarchical mapping of annual global land cover 2001 to present: The MODIS Collection 6 Land Cover product. Remote Sensing of Environment, 222: 183-194.
- 1010 [Song, Y., et al., 2022. Increased global vegetation productivity despite rising atmospheric dryness over the last two decades. Earth's Future, 10, e2021EF002634.](#)
- [Sun, C., Jiang, Z., Li, W., Hou, Q. and Li, L., 2019. Changes in extreme temperature over China when global warming stabilized at 1.5 degrees C and 2.0 degrees C. Scientific Reports, 9\(1\): 14982.](#)
- [Sun et al., 2022. Causes for the increases in both evapotranspiration and water yield over vegetated mainland China during the last two decades. Agricultural and Forest Meteorology, 324, 109118.](#)
- 1015 Tagesson, T. et al., 2020. Recent divergence in the contributions of tropical and boreal forests to the terrestrial carbon sink. Nature Ecology & Evolution, 4(2): 202-209.
- [Thornton, P.E. et al., 2002. Modeling and measuring the effects of disturbance history and climate on carbon and water budgets in evergreen needleleaf forests. Agricultural and Forest Meteorology, 113\(1-4\):185-222.](#)
- 1020 Tong, X. et al., 2018. Increased vegetation growth and carbon stock in China karst via ecological engineering. Nature Sustainability, 1(1): 44-50.
- Viña, A., McConnell, W.J., Yang, H., Xu, Z. and Liu, J., 2016. Effects of conservation policy on China's forest recovery. Science Advances, 2: e1500965.
- 1025 [Wang et al., 2008. Spatiotemporal dynamics of forest net primary production in China over the past two decades. Global and Planetary Change, 61\(3-4\), 267-274.](#)
- Wang, B., Ma, Y., Su, Z., Wang, Y. and Ma, W., 2020a. Quantifying the evaporation amounts of 75 high-elevation large dimictic lakes on the Tibetan Plateau. Science Advances, 6: eaay8558.
- 1030 Wang, M. et al., 2018. Detection of Positive Gross Primary Production Extremes in Terrestrial Ecosystems of China During 1982-2015 and Analysis of Climate Contribution. Journal of Geophysical Research: Biogeosciences, 123(9): 2807-2823.
- Wang, M., Wang, S., Zhao, J., Ju, W. and Hao, Z., 2021a. Global positive gross primary productivity

- extremes and climate contributions during 1982-2016. *Sci Total Environ*, 774: 145703.
- Wang, Q. et al., 2003. Simulation and scaling of temporal variation in gross primary production for coniferous and deciduous temperate forests. *Global Change Biology* 10: 37–51.
- 1035 Wang, R., Chen, J.M., Luo, X., Black, A. and Arain, A., 2019. Seasonality of leaf area index and photosynthetic capacity for better estimation of carbon and water fluxes in evergreen conifer forests. *Agricultural and Forest Meteorology*, 279: 107708.
- Wang, S. et al., 2020b. Estimation of Leaf Photosynthetic Capacity From Leaf Chlorophyll Content and Leaf Age in a Subtropical Evergreen Coniferous Plantation. *Journal of Geophysical Research: Biogeosciences*, 125(2): e2019JG005020.
- 1040 Wang, S., Zhang, Y., Ju, W., Qiu, B. and Zhang, Z., 2021b. Tracking the seasonal and inter-annual variations of global gross primary production during last four decades using satellite near-infrared reflectance data. *Sci Total Environ*, 755(Pt 2): 142569.
- Wang, X., Chen, J.M., Ju, W. and Zhang, Y., 2022. Seasonal Variations in Leaf Maximum Photosynthetic Capacity and Its Dependence on Climate Factors Across Global FLUXNET Sites. *Journal of Geophysical Research: Biogeosciences*, 127(5): e2021JG006709.
- 1045 Wieder, W.R., Bohnert, J., Bonan, G.B. and Langseth, M., 2014. Regridded Harmonized World Soil Database v1.2. ORNL DAAC, Oak Ridge, Tennessee, USA. <https://doi.org/10.3334/ORNLDAAC/1247>.
- 1050 Xiao, Z. et al., 2016. Long-Time-Series Global Land Surface Satellite Leaf Area Index Product Derived From MODIS and AVHRR Surface Reflectance. *IEEE Transactions on Geoscience and Remote Sensing*, 54(9): 5301-5318.
- Xie et al., 2018. Derivation of temporally continuous leaf maximum carboxylation rate (V_{cmax}) from the sunlit leaf gross photosynthesis productivity through combining BEPS model with light response curve at tower flux sites. *Agricultural and Forest Meteorology*, 259(15): 82-94.
- 1055 Xie, S., Mo, X., Hu, S. and Liu, S., 2020. Contributions of climate change, elevated atmospheric CO₂ and human activities to ET and GPP trends in the Three-North Region of China. *Agricultural and Forest Meteorology*, 295: 108183.
- Xie, X. et al., 2019. Assessment of five satellite-derived LAI datasets for GPP estimations through ecosystem models. *Science of the Total Environment*, 690: 1120-1130.
- 1060 Xu, M. et al., 2022. A 21-Year Time Series of Global Leaf Chlorophyll Content Maps From MODIS Imagery. *IEEE Transactions on Geoscience and Remote Sensing*, 60: 1-13.
- [Xu, C. et al., 2019. Increasing impacts of extreme droughts on vegetation productivity under climate change. *Nature Climate Change*, 9, 948–953.](#)
- 1065 Yang, F. et al., 2017a. Evaluation of multiple forcing data sets for precipitation and shortwave radiation over major land areas of China. *Hydrology and Earth System Sciences*, 21(11): 5805-5821.
- Yang, Y., Xiao, P., Feng, X. and Li, H., 2017b. Accuracy assessment of seven global land cover datasets over China. *ISPRS Journal of Photogrammetry and Remote Sensing*, 125: 156-173.
- Yao, Y., Piao, S. and Wang, T., 2018a. Future biomass carbon sequestration capacity of Chinese forests. *Science Bulletin*, 63(17): 1108-1117.
- 1070 Yao, Y. et al., 2018b. Spatiotemporal pattern of gross primary productivity and its covariation with climate in China over the last thirty years. *Global Change Biology*, 24(1): 184-196.
- Yin, R. and Yin, G.J.E.M., 2010. China's Primary Programs of Terrestrial Ecosystem Restoration:

Initiation, Implementation, and Challenges. *Environmental Management* 45(3): 429-441.

- 1075 Yu, D.Y. et al., 2011. Forest ecosystem restoration due to a national conservation plan in China. *Ecological Engineering*, 37(9): 1387-1397.
- Yu, G.-R. et al., 2006. Overview of ChinaFLUX and evaluation of its eddy covariance measurement. *Agricultural and Forest Meteorology*, 137(3-4): 125-137.
- 1080 Yu, G. et al., 2014. High carbon dioxide uptake by subtropical forest ecosystems in the East Asian monsoon region. *Proceedings of the National Academy of Sciences*, 111(13): 4910-4915.
- Yuan, W. et al., 2016. Severe summer heatwave and drought strongly reduced carbon uptake in Southern China. *Scientific Reports*, 6(1): 18813.
- [Yuan, W. P., et al., 2019. Increased atmospheric vapor pressure deficit reduces global vegetation growth. *Science Advances*, 5, eaax1396.](#)
- 1085 ~~Zhan, C. et al., 2022. Emergence of the physiological effects of elevated CO₂ on land-atmosphere exchange of carbon and water. *Global Change Biology*, 28(24): 7313-7326.~~
- Zhang, F. et al., 2012. Variations of Terrestrial Net Primary Productivity in East Asia. *Terrestrial, Atmospheric and Oceanic Sciences*, 23(4): 425-437.
- 1090 Zhang, X. et al., 2022. Land cover change instead of solar radiation change dominates the forest GPP increase during the recent phase of the Shelterbelt Program for Pearl River. *Ecological Indicators*, 136: 108664.
- Zhang, Y. et al., 2014. Effects of land use/land cover and climate changes on terrestrial net primary productivity in the Yangtze River Basin, China, from 2001 to 2010. *Journal of Geophysical Research: Biogeosciences*, 119(6): 1092-1109.
- 1095 Zhang, Y. et al., 2017. A global moderate resolution dataset of gross primary production of vegetation for 2000-2016. *Scientific Data*, 4: 170165.
- Zheng, Y. et al., 2020. Improved estimate of global gross primary production for reproducing its long-term variation, 1982–2017. *Earth System Science Data*, 12(4): 2725-2746.
- [Zhu, et al., 2016. Greening of the Earth and Its Drivers. *Nature Climate Change*, 6 \(8\): 791–795.](#)
- 100 [Zhu et al., 2017. Attribution of seasonal leaf area index trends in the northern latitudes with “optimally” integrated ecosystem models. *Global Change Biology*, 23, 4798–4813.](#)